UNLV Retrospective Theses & Dissertations

1-1-2006

Computational modeling of proton exchange membrane electrolysis cell for hydrogen production

Shanthi P Katukota
University of Nevada, Las Vegas

Follow this and additional works at: https://digitalscholarship.unlv.edu/rtds

COMPUTATIONAL MODELING OF PROTON EXCHANGE MEMBRANE

ELECTROLYSIS CELL FOR HYDROGEN PRODUCTION

by

Shanthi P Katukota

Bachelor of Engineering in Mechanical Engineering
Osmania University, India
2004

A thesis submitted in partial fulfillment
of the requirements for the

Master of Science Degree in Mechanical Engineering
Department of Mechanical Engineering
Howard R. Hughes College of Engineering

Graduate College
University of Nevada, Las Vegas
December 2006

UMI Number: 1441713

INFORMATION TO USERS

The quality of this reproduction is dependent upon the quality of the copy submitted. Broken or indistinct print, colored or poor quality illustrations and photographs, print bleed-through, substandard margins, and improper alignment can adversely affect reproduction.

In the unlikely event that the author did not send a complete manuscript and there are missing pages, these will be noted. Also, if unauthorized copyright material had to be removed, a note will indicate the deletion.

UMI®

UMI Microform 1441713

Copyright 2007 by ProQuest Information and Learning Company.

All rights reserved. This microform edition is protected against unauthorized copying under Title 17, United States Code.

ProQuest Information and Learning Company
300 North Zeeb Road
P.O. Box 1346
Ann Arbor, MI 48106-1346

UNLV
UNIVERSITY OF NEVADA LAS VEGAS

Thesis Approval
The Graduate College
University of Nevada, Las Vegas

_____3rd November____, 20_06_

The Thesis prepared by

Shanthi P. Katukota _____

Entitled

Computational Modeling of Proton Exchange Membrane Electrolysis Cell

for Hydrogen Production _____

_____

is approved in partial fulfillment of the requirements for the degree of

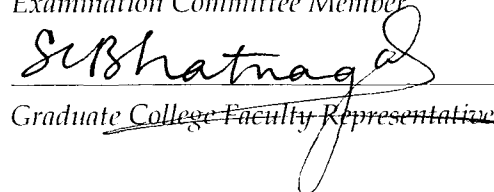Master of Science in Mechanical Engineering_____

_____
Examination Committee Chair

_____
Dean of the Graduate College

_____
Examination Committee Member

_____
Examination Committee Member

_____ 11/03/06
Graduate College Faculty Representative

1017-53

ii

ABSTRACT

**Computational Modeling of Proton Exchange Membrane Electrolysis Cell
for Hydrogen Production**

by

Shanthi P Katukota

Dr. Yitung Chen, Examination Committee Chair
Associate Professor of Department of Mechanical Engineering
University of Nevada, Las Vegas

Numerical simulations of electrochemical process for hydrogen production were performed for the purpose of examining the phenomena occurring within the proton exchange membrane (PEM) water splitting cell. A steady-state isothermal two-dimensional model of the cell is developed. Finite element method was used to solve the multi-component transport model coupled with flow in porous medium, charge balance and electrochemical kinetics.

Parametric studies were performed based on appropriate mass balances, transport, and electrochemical kinetics applied to the cell. It is observed that, as the water on the anode side flows from the inlet to the outlet, the mass fraction of oxygen increases because of the oxidation of oxygen. Similarly, on the cathode side, as the mass fraction of water decreases, the hydrogen mass fraction increases resulting in the formation of hydrogen by reduction of protons. Effects of cell temperature, length of the current

iii

collector and thickness of the membrane on the cell performance are examined. As the cell temperature increases, the current density across the cell and mass fraction of hydrogen increases respectively. Increase in thickness of membrane causes a decrease in the cell current density. The current density across the cell tends to increase as the length of the current collector increases.

TABLE OF CONTENTS

v

TABLE OF FIGURES

ACKNOWLEDGEMENTS

I express my sincere gratitude to Dr. Yitung Chen and Dr. Robert F Boehm for their continuous guidance, support and encouragement throughout this research activity.

I would also like to thank Dr. Jianhu Nie and Dr. Hsuan-Tsung (Sean) Hsieh for their support and co-operation throughout this program.

I would like to thank Dr. Satish C Bhatnagar for his time in reviewing the prospectus, participation of defense as the committee member.

I would like to thank the U.S. Department of Energy and University of Nevada, Las Vegas for their continuous support throughout the entire research work.

Finally, I would like to thank my Appaji (Sri Ganapati Sachchidananda Swamiji), parents and friends, without their continuous support and faith this work would not have been possible.

CHAPTER 1

INTRODUCTION

1.1 The global picture

Transforming today's non-sustainable energy usage into a globally sustainable energy economy is one of mankind's key challenges for the current century. This transformation process encompasses a multitude of different aspects – technological, social, and economical.

It involves abandoning or changing energetically aberrant habits. Why is a mass of 1.5 tonnes displaced to transport one person for a couple of kilometers? Why is food transported around the globe when similar products are available locally? It involves energy prices reflecting a true and sustainable cost instead of excavation, transport and tax.

It involves technological advances to increase the efficiency of energy transformation and storage processes. It involves technological advances to develop more energy efficient transportation systems and housing. While social and economical changes present a huge and sadly so far untapped – potential in the reduction of current energy consumption, it is not enough. Technological advances are required to be able to successfully use renewable as a primary energy source. The reason lies in the stochastic

1

nature of many renewable energy sources (i.e. wind or solar power) as well as their limited availability. Technological advances therefore need to provide solutions to the following three problems:

a) Efficient energy conversion

b) Energy storage

c) Extraction of energy

The various paths to hydrogen production are depicted in the Figure 1.1. The extra steps between the energy source and hydrogen correspond to mean efficiency loss and/or long-term environmental costs. Direct solar electrolysis can be over 27% more efficient than solar photo-voltaic linked with a separate electrolyzer. In 2005, the world produced 425 quad BTU (10^{15} BTU) from petroleum (primary level), coal, natural gas, nuclear fission, and renewable sources (hydroelectric, biomass, geothermal, solar, and wind). The following breakdown in terms of percentage is depicted in Figure 1.2.

2
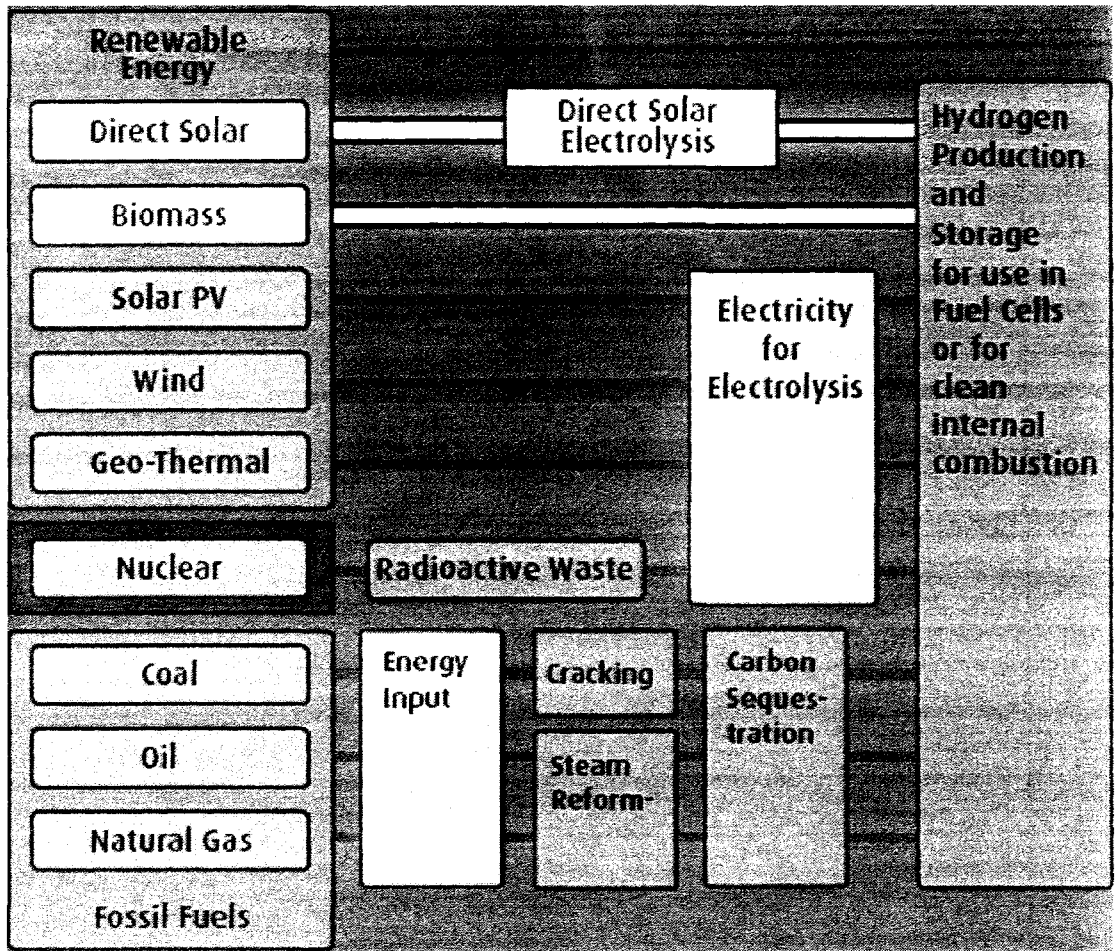
Figure 1.1: Various paths to hydrogen production [5]
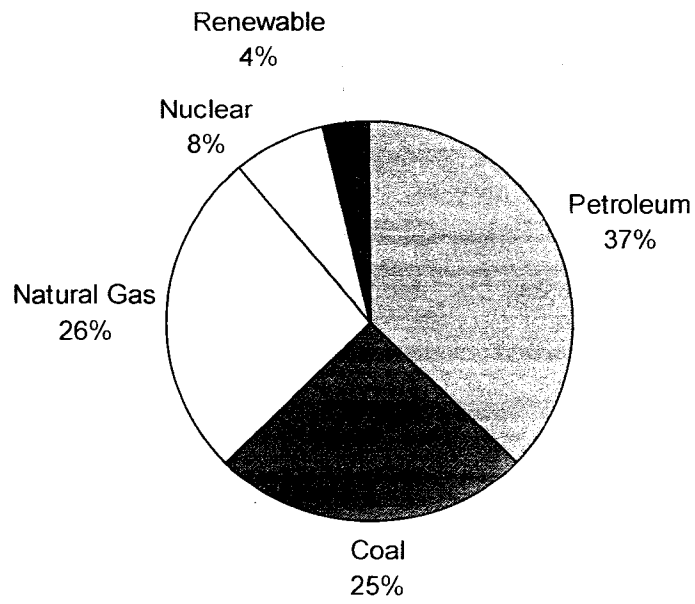
(a) Total energy distribution in the year 2005
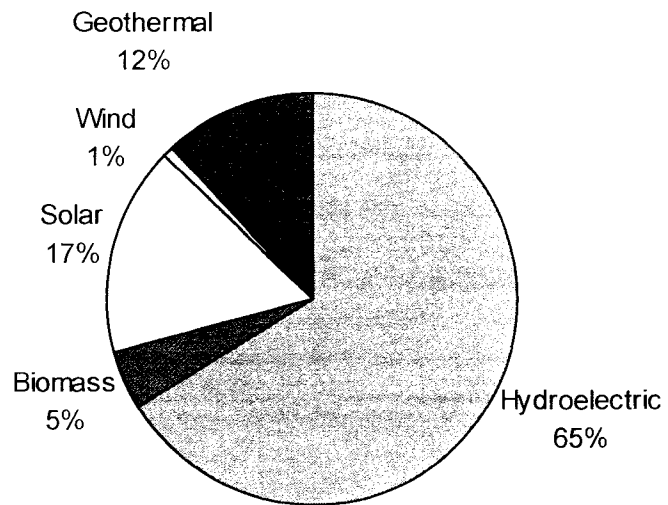
(b) Renewable energy distribution in the year 2005

Figure 1.2: The world energy scenario, 2005 [6]

4

1.2 Historical development of hydrogen production

The United State's rapid economic expansion during the 1950s and 1960s created a huge market for energy suppliers. While domestic production of coal remained constant during the postwar expansion, usage of nuclear power, oil, and natural gas increased substantially. Oil consumption increased from 10 quads (Quad is a unit of energy equivalent to 10^{15} BTU) in 1945 to 30 quads in 1970 and natural gas consumption increased from 4 quads to 22 quads during the same period [1].

Awareness of the environmental and human health risks associated with large scale fossil fuel use pinnacled in the 1960s and 70s. Air pollution in large metropolitan areas such as Los Angeles typified the concerns of vocal segments of the U.S. population. In addition to environmental problems, the Organization of Petroleum Exporting Countries (OPEC) oil embargo of 1973 helped to catapult oil prices from $1.40 per barrel in 1970 to more than $8 per barrel in 1974 [1]. The price of oil was under $25 per barrel in September 2003. By August 11, 2005, the price had been above $60 per barrel for over a week and a half. A record price of $78.40 per barrel was reached on July 13, 2006, due in part to North Korea's missile launches, Middle East Crisis, Iranian nuclear brinkmanship and reports from the U.S. Department of Energy showing a decline in petroleum reserves. Pressure on the U.S. government to find a long-term solution to all these problems spurred the Solar Energy Research Development and Demonstration Act of 1974, which funded large-scale research in alternative fuels and energy sources, including hydrogen energy.

5

1.3 The hydrogen economy

The vision of hydrogen as a replacement for fossil fuels did not become popularized until the first international meeting on hydrogen energy, the Hydrogen Economy Miami Energy Conference, in 1974 [2]. In addition to generating a large interest in hydrogen energy, the conference introduced the term "hydrogen economy" into the dialogue of energy production. As outlined in the conference, a hydrogen economy is an energy infrastructure in which the sun's energy is used to produce hydrogen. The hydrogen stores the sun's energy; in the same way that coal or oil also stores the sun's energy (sunlight produces plant matter, which slowly turns into coal or oil deposits). When electricity is needed, the hydrogen is burned (also analogous to how coal or oil is burned to produce electricity).

The hydrogen economy is an attractive solution to the U.S. energy problems for several reasons. First, very little pollution is produced in the hydrogen economy. Both the production and the burning of hydrogen produce no pollution (water is the only byproduct of burning hydrogen). Second, the hydrogen economy is extremely efficient in terms of converting the sun's energy into a useable form of electricity. Third, nearly all of the resources needed for a hydrogen economy are found in the U.S., so there will not be an opportunity for another energy embargo caused by foreign suppliers. Finally, the hydrogen economy is a long-term solution. Because the hydrogen economy is driven only by sunlight, the hydrogen economy will last as long as the sun continues to shine.

The first of the three main goals in the hydrogen economy is to produce hydrogen cleanly, efficiently, and renewably. Although hydrogen is the most abundant element in the universe, it is usually not found on the earth in a usable form (as the H_2 molecule). In

6

order to use hydrogen, it must be extracted from hydrogen-containing materials (such as water or plant matter) before it can be used. An input of energy must be used to extract H_2 from hydrogen-containing materials. Hydrogen can be produced using fossil fuels via steam reforming or partial oxidation of natural gas and by coal gasification. Produced in this fashion, hydrogen will generate less CO_2 than conventional internal combustion engines [3]. It can also be produced via electrolysis using electricity and water. Nuclear power can provide the energy for hydrogen production by a variety of means, but has several disadvantages. Some thermo-chemical processes, such as the sulfur-iodine cycle (S-I cycle), can produce hydrogen and oxygen from water and heat without using electricity. Since all the input energy for such processes is heat, they can be more efficient than high-temperature electrolysis. Thermo-chemical production of hydrogen using chemical energy from coal or natural gas is generally not considered, because the direct chemical path is more efficient. An extremely attractive way of providing this energy is in a clean and renewable fashion by using solar and wind power.

The second goal in the hydrogen economy is to efficiently and safely store and transport the hydrogen once it is produced. The science behind transporting hydrogen is a trivial matter: because hydrogen gas has similar properties to natural gas, hydrogen can be transported through pipelines in a way similar to natural gas. Storing hydrogen efficiently, however, is a difficult challenge. Traditionally, hydrogen has been stored under high pressure in thick-walled metal tanks. This is inefficient, because pressurizing hydrogen requires substantial energy inputs. One method currently being explored for hydrogen storage makes use of the "capillary effect" – the way that water is drawn

7

upwards in a narrow capillary tube and second method is the use of metal hydrides, in which hydrogen is adsorbed onto thin metal plates.

The third goal in the hydrogen economy is to efficiently extract energy from hydrogen. A device called a fuel cell carefully combines hydrogen with oxygen (this is the process of burning). When hydrogen combines with oxygen in a fuel cell, electricity from the reaction can be used to run an electric motor. Although there are a wide variety of fuel cells currently in use, there is much research underway on improving the long-term stability of fuel cells.

Important breakthroughs have been made in each of the three main areas of the hydrogen economy since the first international hydrogen conference in 1974. The remainder of this thesis will focus on the first area – that of hydrogen production.

1.4 Renewable hydrogen production

As mentioned previously, an input of energy is needed to extract H_2 from hydrogen-containing compounds, since hydrogen does not occur by itself in nature. There are multiple sustainable paths to producing hydrogen, all of which begin with solar energy [4].

- *Wind turbine and water electrolyzer:* Solar energy heats the surface of the earth, generating wind currents, which turn a wind turbine. The wind turbine produces electricity, which is fed into water via a water electrolyzer. The water electrolyzer is a device capable of sending large currents of electricity through water to split the water into hydrogen and oxygen.

- *Photovoltaic panel and water electrolyzer:* Energy from sunlight is captured on a photovoltaic panel. The photovoltaic panel produces electricity (electrons) and

8

feeds it to a water electrolyzer, producing hydrogen and oxygen gasses. This is about half as efficient as direct photo-electrolysis, because there are a large number of metal contacts on the photovoltaic panel that increase electrical resistance.

- *Low temperature pyrolysis:* Biomass that has grown with the aid of sunlight is heated in the absence of oxygen. This converts the biomass into oil, from which hydrogen can be extracted. This method of hydrogen production does produce some pollution, in the form of carbon dioxide and carbon monoxide.

- *Photo-biological methods:* Photosynthetic microbes in water produce hydrogen as part of their metabolic activities when light is shined on them.

- *Direct photo-electrolysis:* Sunlight hits a photovoltaic panel that is immersed in water. Electrons (electricity) directly enter the water from the photovoltaic panel, allowing a highly efficient transfer of energy. The electrons provide the energy to split water into hydrogen.

The last method, direct photo-electrolysis, has the potential to be the most efficient method of hydrogen production. While the photovoltaic panel and water electrolyzer systems achieve maximum 4-6% efficiency, direct photo-electrolysis systems have achieved 12% efficiency (National Renewable Energy Laboratory, 1998).

1.5 The photo-electrochemical water splitting process

A photo-electrochemical (PEC) system combines the harvesting of solar energy with the electrolysis of water. When a semiconductor of the proper characteristics is immersed in an aqueous electrolyte and irradiated with sunlight, the energy can be sufficient to split water into hydrogen and oxygen. Depending on the type of

9

semiconductor material and the solar intensity, this current density is 10-30 mA/cm^2. At these current densities, the voltage required for electrolysis is much lower, and therefore, the corresponding electrolysis efficiency is much higher. At a current density similar to short-circuit photocurrent from an ideal PEC water splitting system, hydrogen and oxygen generation is achieved at an effective applied voltage of approximately 1.35 V, giving rise to an electrolysis efficiency of 91%. One of the major advantages of a direct conversion photo-electrochemical system is that it not only eliminates most of the costs of the electrolyzer, but it also has the possibility of increasing the overall efficiency of the process leading to a further decrease in costs.

For direct photo-electrochemical decomposition of water to occur, several key criteria of the semiconductor must be met: the semiconductor system must generate sufficient voltage to split water, the energetic of the semiconductor must overlap that of the hydrogen and oxygen redox reactions, the semiconductor system must be stable in aqueous electrolytes, and finally the charge transfer from the surface of the semiconductor must be fast enough not only to prevent corrosion but also reduce energy losses due to over-voltage.

A diagram of a water splitting cell and its pertinent electron energy levels for both n-type and p-type semiconductors is shown in Figure 1.3. In part (a), a catalyzed semiconductor photo-electrode is ohmically contacted to a catalytic counter electrode, and the two are immersed in an aqueous solution. Under illumination, hydrogen is produced at one electrode and oxygen is produced at the other. Which gas is produced at which electrode is determined by the direction of charge carrier flow in the cell. Part (a) of the figure indicates the gas evolution reactions for n-type material in an acid solution.

10

Part (b) of Figure 1.3 shows simple energy diagrams for n-type and p-type cells at equilibrium (no illumination, no applied potentials, and electrical continuity throughout the cell). In each of the band diagrams, the upper solid line indicates the conduction band edge energy, the dotted line indicates the Fermi energy, and the lower solid line indicates the valence band edge energy. A Schottky junction at the semiconductor/solution interface creates a charge depletion region at equilibrium, and it is the direction of the band bending in this region that determines the direction of charge carrier flow under illumination.

At equilibrium, the Fermi energy is constant throughout the semiconductor. The band bending at equilibrium is created by the difference in the energy of the band edges relative to the Fermi level in the bulk and at the surface of the material. For the semiconductor bulk, the band edge position relative to the Fermi level is a function of the majority carrier concentration, which can be controlled by altering the dopant concentration. The addition of n-type dopant brings the conduction band close to the Fermi level, whereas the addition of p-type dopants brings the valence band close to the Fermi level. For semiconductor surfaces, however, the location of the band edges relative to the Fermi level is often nearly independent of the bulk doping. The band edge positions at the material surface relative to the Fermi level are a function of the density and occupation of electron states at the material surface. These surface states are caused by un-terminated bonds, reconstruction at the crystal surface, and interactions between the surface atoms and the solution. Typically, the position of the band edges at the surface relative to the Fermi level can only be modified by surface treatments that change the occupation or density of the electron surface states. For non-illuminated n-type

11

material with its surface Fermi level pinned near the middle of its band gap, the valence and conduction bands bend upward in electron energy as they approach the semiconductor/solution interface. When photons are absorbed in the depletion region to generate electron-hole pairs, the holes are driven to the semiconductor/solution interface and the electrons are driven to the counter electrode/solution interface. Under intense illumination, sufficient charge carriers can be photo-generated to flatten the band bending and move the bulk Fermi level above the surface Fermi level. This is depicted in part (c) of Figure 1.3. If the bulk Fermi level, which is identical to the Fermi level in the counter electrode, becomes higher in energy than the hydrogen-producing half-reaction, electrons in the counter electrode can transfer to the solution to produce hydrogen. If the valence band edge at the semiconductor surface is lower in energy than the oxygen-producing half-reaction, holes reaching the semiconductor/solution interface can accept an electron from the solution to produce oxygen.

For non-illuminated p-type material with its surface Fermi level pinned near the middle of its band gap, the bands bend downward as they approach the semiconductor/solution interface. In this case, photo-generated electrons are driven to the semiconductor/solution interface, photo-generated holes are driven toward the counter electrode/solution interface, and illumination causes the bulk Fermi level to drop below the surface Fermi level. If the bulk Fermi level drops below the oxygen-producing half-reaction, electrons can transfer from the solution to the counter electrode to produce oxygen. If the conduction band edge at the semiconductor surface is higher in energy than the hydrogen-producing half-reaction, electrons can transfer from the semiconductor to the solution to produce hydrogen.
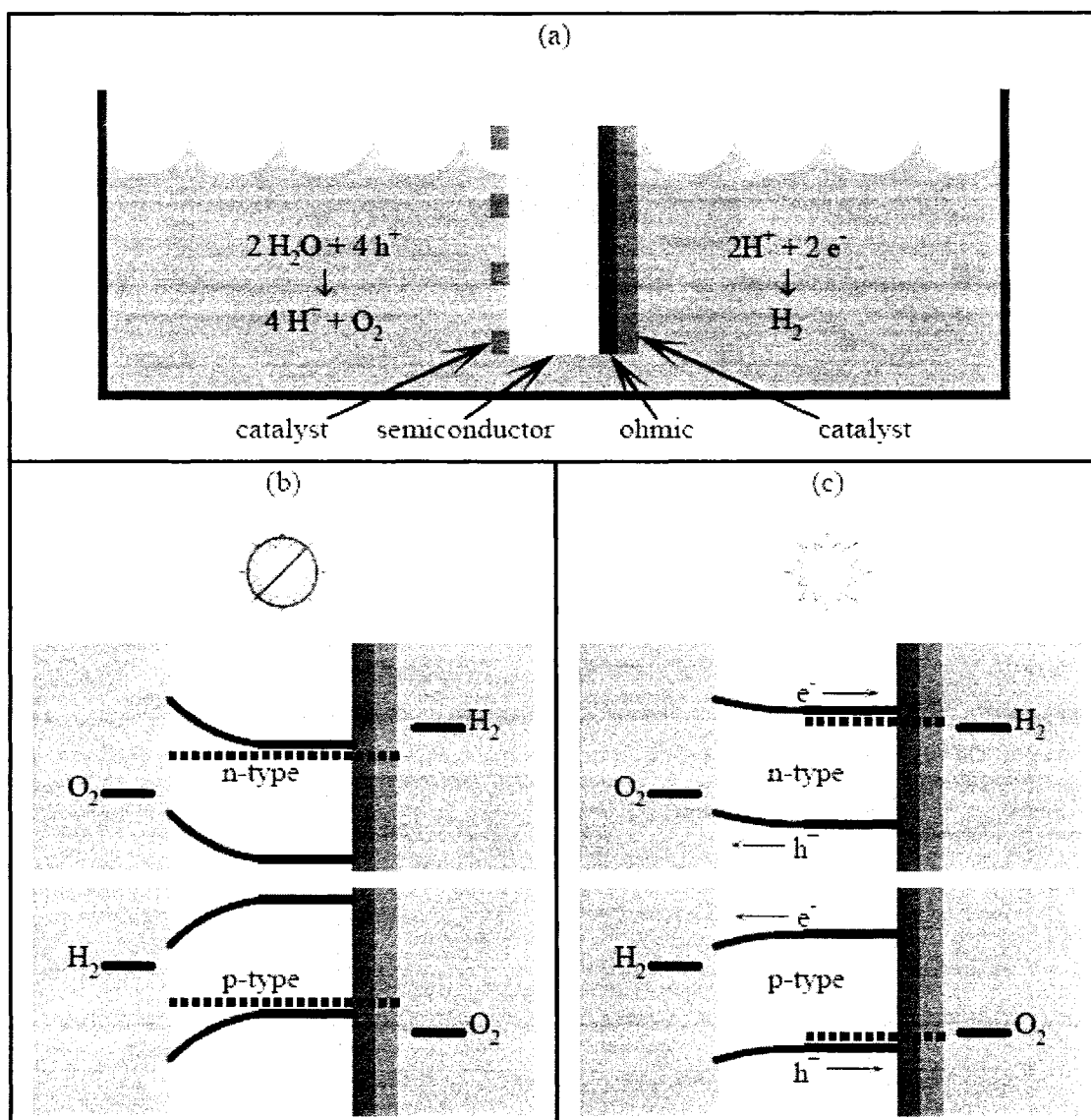
Figure 1.3: A schematic diagram of a water splitting cell (a) in an acid solution and band diagrams for n-type and p-type cells (b) in darkness and (c) light [7].

1.5.1 Water splitting photo-electrode material requirements

A semiconductor that is to be used as a water splitting photo-electrode must meet several requirements related to its band gap, electronic energies, and chemical stability. In short, its band gap needs to be approximately 1.8 eV, its electron-accepting and

13

electron-donating states need to "straddle" the hydrogen and oxygen production potentials, and it needs to be sufficiently stable that it is not damaged by the water splitting environment. These requirements will be explained more fully in the following paragraphs.

The ideal band gap for a single photo-electrode cell is determined by a trade-off between maximizing the absorption of solar photons and generating the required energy to drive the water splitting reactions. Maximum solar absorption is attained by minimizing the semiconductor band gap. However, if the band gap becomes too small, the cell will not generate the potential required to drive the water splitting reactions. The potential difference between the hydrogen-producing half-reaction and the oxygen-producing half-reaction is 1.229 V. The oxygen producing half-reaction typically requires an additional 0.275 V over-potential and the hydrogen-producing half-reaction requires an additional 0.050 V over-potential to proceed at a reasonable rate [8]. For a single-photo-electrode cell, either the cell's electron-accepting state or its electron-donating state is at the bulk Fermi energy, which is typically 0.050-0.200 eV from a band edge depending upon the material doping. These all result in the requirement that the semiconductor band gap be approximately 1.8 eV for a single photo-electrode water splitting cell [9, 10].

Besides having the proper band gap, the electron-donating and electron-accepting states for the water splitting cell must have the appropriate potentials to drive the water splitting reactions. At the semiconductor surface, electron donation comes from the conduction band edge (p-type materials) or electron acceptance comes from the valence band edge (n-type materials). The position of the band edges at the semiconductor surface

14

relative to the half-reaction energies in the solution is dictated by the electric field generated by ions or dipoles adsorbed on the semiconductor surface and by the semiconductor band edge positions relative to the surface Fermi level. At the counter electrode surface, either electron donation or electron acceptance comes from the Fermi level. When the cell is illuminated, the counter electrode Fermi level relative to the half-reaction energies in solution is dictated by a combination of the adsorption layer on the semiconductor surface and the photo-voltage developed in the semiconductor bulk.

To have a long device lifetime, the semiconductor must have sufficient electrochemical stability that the charge carriers arriving at its surface drive only the water splitting reactions, and not electrode corrosion reactions. For p-type materials, the electrons arriving at the semiconductor surface can either transfer to the solution to drive the hydrogen-producing half-reaction, recombine harmlessly via surface recombination centers, or drive semiconductor reduction reactions (for example, reducing a metal oxide to a metal). For n-type materials, the holes arriving at the semiconductor surface can either accept an electron from solution to drive the oxygen-producing half-reaction, recombine harmlessly via surface recombination centers, or drive semiconductor oxidation reactions. In general, semiconductors are much more resistant to reduction reactions than oxidation reactions, making p-type material more stable than n-type material. The stability of both types of material is enhanced by catalytic surface treatments, which increase the rate of charge transfer from the semiconductor surface to the solution. If the charge carriers are transferred to the solution as quickly as possible, their possibility of participating in recombination or corrosion is minimized.

15

1.5.2 A review of previously examined photo-electrode materials

A variety of semiconductors have been tested as water splitting photo-electrodes, but none examined thus far meet all of the requirements to be optimal. Wide band gap semiconductors such as TiO_2 [11] and $SrTiO_3$ [12, 13] have the appropriate band edge energies for water splitting and have good photo-electrochemical stability, but their band gaps are too large to absorb a reasonable fraction of the solar spectrum. $Al_xGa_{1-x}As$ can be grown with the ideal 1.8 eV band gap, but the arsenides etch easily in both acidic and basic solutions in darkness. p-InP has been shown to be photo-electrochemically stable in acid, but its 1.4 eV band gap is too small for single-photo-electrode applications; it requires an external bias to split water [14, 15]. $p-In_{0.5}Ga_{0.5}P$ has an ideal band gap, but its illuminated bulk Fermi level is too high in energy to drive the oxygen-producing half-reaction [16]. A $p-In_{0.5}Ga_{0.5}P$-GaAs tandem cell utilizing a buried GaAs p-n junction to lower the energy of the counter electrode has been shown to operate at 12.4% efficiency [17], but such a growth process is expensive and the cell's performance decays over time, possibly due to reduction of the oxide layer at the $p-In_{0.5}Ga_{0.5}P$ surface.

1.6 Electrolyzers

The electrolyzer is a device that generates hydrogen and oxygen from water through the application of electricity and consists of a series of porous graphite plates through which water flows while low voltage direct current is applied.

Electrolyzers split the water into hydrogen and oxygen gases by the passage of electricity, normally by breaking down compounds into elements or simpler products. An electrolyzer has to fulfill requirements such as high efficiency, low cost, large range of operation etc. Physically a practical electrolyzer stack will consist of several cells linked

16

in series. Mono-polar and bipolar are two types of cell designs. A mono-polar design is when the electrodes are either negative or positive with parallel electrical connection of the individual cells as shown in Figure 1.4.
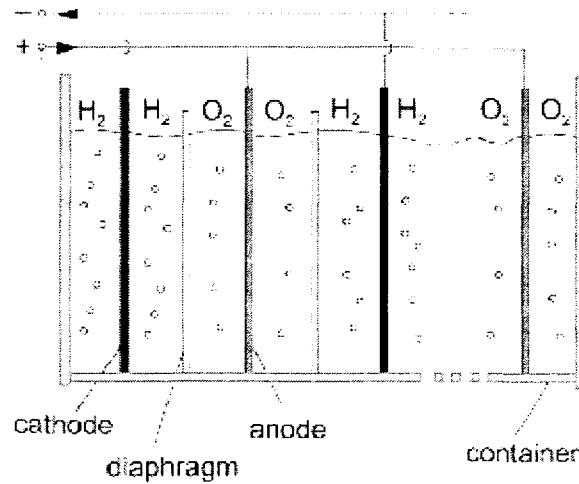
Figure 1.4: Mono-polar Design [18]

In a bipolar design the individual cells are linked in series electrically and geometrically as shown in Figure 1.5.
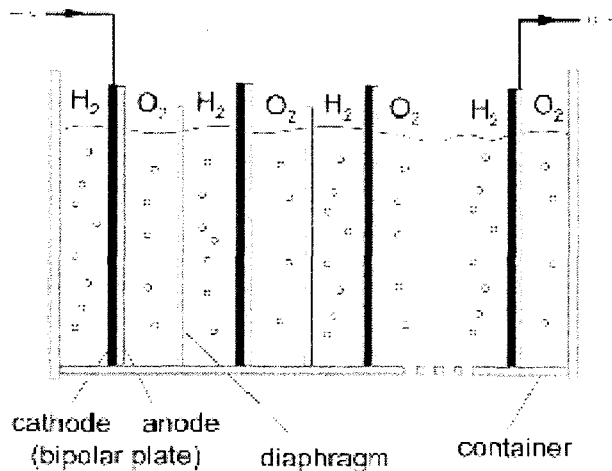
Figure 1.5: Bipolar Design[18]

17

An advantage of the bipolar electrolyzer stack design is that it is more compressed than the mono-polar design. This means that the length of the electrical wires is minimized and the losses due to the internal ohmic resistance of the electrolyte is reduced therefore the electrolyzer efficiency is increased.

On the other hand, there are also some disadvantages with bipolar cells design. One of these is the corrosion problem that can occur because of parasitic currents. This current is caused by parasitic elements of the electric circuit and it can lead to losses of electrical energy. Furthermore, the compactness and high pressures of the bipolar electrolyzers, which can result in large quantities of hydrogen and oxygen can being generated in a small unit with small space requirement, involve relatively sophisticated and complex system designs. This means that the manufacturing cost is increased. The relatively simple and sturdy mono-polar electrolyzer systems are in comparison less costly to manufacture [19].

1.7 Types of electrolyzers

1.7.1 Alkaline electrolyzer

Alkaline water electrolyzers usually use electrolyte that contains aqueous potassium hydroxide (KOH), mostly with solutions of 20-30 wt% because of the optimal conductivity and require using corrosion resistant stainless steel to withstand the chemical attack. The typical operating temperatures and pressures of these electrolyzers are 70–100 °C and 1–30 bar respectively. The chemical reactions that take place in the operation of the alkaline electrolyzer are mentioned below.

For the cathode reaction it is:

$$4OH^- \longrightarrow O_2 + 4e^- + 2H_2O \tag{1}$$

18

For the anode reaction it is:

$$4H_2O + 4e^- \longrightarrow 2H_2 + 4OH^- \tag{2}$$

And finally the overall reaction is:

$$2H_2O \longrightarrow 2H_2 + O_2 \tag{3}$$
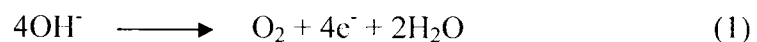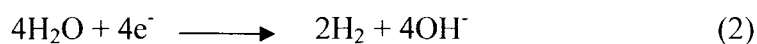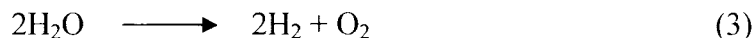
1.7.2 Proton exchange membrane electrolyzer

Polymer electrolyte membranes [PEMs] were first developed for the chlor-alkali industry. These specialized materials, also known as ionomers, are solid fluoro-polymers which have been chemically altered to make them electrically conductive. The fluorocarbon chain or backbone has typically a repeating structural unit, such as - $[CF_2$. $CF_2]_{n-}$, where n is very large. Treatments like sulphonation or carboxylation, insert ionic or electrically-charged pendant groups, statistically spaced, into some of these base units giving, e.g., - $[CF(SO_3$. $H+)$ ¾ $CF2]_{m-}$, where m can range from n/5 to n/20 depending on the properties most suited for the application. Nafion[R], made by Du Pont, is the most commercially successful of such materials, and is available as thin pre-formed membranes in various thicknesses, or as a 5 % solution which may be deposited and evaporated to leave a polymer layer of customized shape.

By coincidence, the letters PE in PEM can stand for "Polymer Electrolyte" or "Proton Exchange" because the last process is linked to the conductivity. Unfortunately, these terms are used interchangeably leading to some confusion for the layman. What is worse, PEM and SPE (Solid Polymer Electrolyte) are also used interchangeably, but the key point is that they all refer to the nafion-type ionomer or its family of compounds [20]. The electrolyzers that are based on Polymer – Electrolyte Membrane (PEM) separators

19

are mostly used for industrial purposes because they can achieve high efficiencies. These devices anticipate the imminent development of a renewable energy economy based on electricity and H_2 fuel as complementary energy vectors.

1.7.3 Polymer electrolyte membrane electrolyzer operation functions

For a PEM electrolyzer, its efficiency is a function primarily of membrane and electro catalyst performance. This becomes crucial under high-current operation, which is necessary for industrial-scale application. The following reactions occur in this electrolyzer:

For the cathode reaction it is:

$$4H^+ + 4e^- \longrightarrow 2H_2 \qquad (4)$$

For the anode reaction it is:

$$2H_2O \longrightarrow 4H^+ + 4e^- + O_2 \qquad (5)$$

And finally the overall reaction is:

$$2H_2O \longrightarrow 2H_2 + O_2 \qquad (6)$$
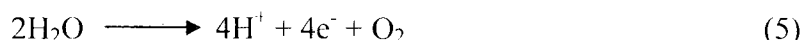
1.7.3.1 Membrane

The membrane consists of solid fluoro-polymer which has been chemically altered in part to contain sulphonic acid groups, SO_3H, which easily release their hydrogen as positively-charged atoms or protons [H^+] [18]:

$$SO_3H \longrightarrow SO_3^- + H^+ \qquad (7)$$
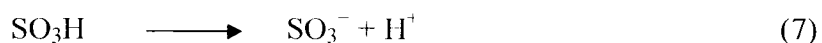
These ionic or charged forms allow water to penetrate into the membrane structure but not the product gases, molecular hydrogen [H_2] and oxygen [O_2]. The resulting hydrated proton, H_3O^+, is free to move whereas the sulphonate ion [SO_3^-] remains fixed to the

20

polymer side-chain. Thus, when an electric field is applied across the membrane the hydrated protons are attracted to the negatively charged electrode, known as the cathode. Since a moving charge is identical with electric current, the membrane acts as a conductor of electricity. It is said to be a protonic conductor. A typical membrane material that is used is called "Nafion". Nafion is a per fluorinated polymer that contains small proportions of sulfonic or carboxylic ionic functional groups. Its general chemical structure contains: X is either a sulfonic or carboxylic functional group or M is either a metal cation in the neutralized form or an H^+ in the acid form. This can be seen in Fig 1.6.

$$(CF_2CF_2)_a \text{---} (CFCF_2)_b$$
$$|$$
$$O$$
$$|$$
$$CF_2$$
$$|$$
$$F-C \text{---} CF_2CF_2 \text{---} X^-M^+$$
$$|$$
$$CF_3$$
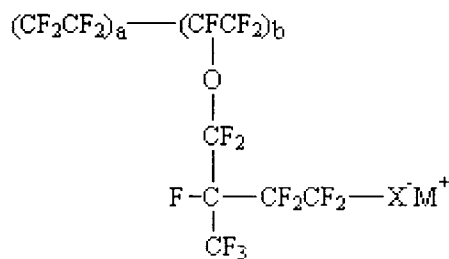
Figure 1.6: Nafion per fluorinated ionomer

It has several advantages over conventional electrolyzers, which normally use an aqueous caustic solution for workable conductivity. Because "Nafion" is a solid, its acidity is self-contained and so chemical corrosion of the electrolyzer housing is much less problematic. Furthermore as it is an excellent gas separator, allowing water to permeate almost to the exclusion of H_2 and O_2 it can be made very thin, typically only 100 microns, or one tenth of a millimeter. This also improves its conductivity so that the electrolyzer can operate efficiently even at high currents. However, the membrane also

21

has some disadvantages. Unlike conventional polymers which are water-repellent, it must also be kept humidified constantly otherwise its conductivity deteriorates and it is a very expensive material. To be kept constantly humidified is never a serious problem in an electrolyzer because of continual contact with water, but the PEM fuel cell requires intensive water management for stable, continuous operation.

1.7.3.2 Electro catalysts

A voltage of about 1.5V is supplied to the metal plate electrodes and a unidirectional (DC) electric current is caused to flow. Protons are drawn to the cathode and are discharged as H atoms by combination with electrons at the metal cathode surface. Pairs of adsorbed H atoms then combine to make molecules of H_2 gas, which escape freeing the electrode surface for more proton discharge:

$$4M + 4H^+ + 4e^- \longrightarrow 4M-H \qquad (8) [20]$$

$$4M-H \longrightarrow 4M + 2H_2 \qquad (9) [20]$$

At the positive electrode or anode, electrons are lost by incoming water molecules creating O atoms and protons. The electrons are shunted to the cathode, protons enter the membrane, and two O atoms combine the release O_2 gas:

$$2M + 2H_2O \longrightarrow 2M-O + 4 H^+ + 4e^- \qquad (10)$$

$$2M-O \longrightarrow 2M + O_2 \qquad (11)$$

22
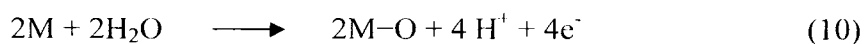
Although the overall process or mechanism is complex, its sum or balance is simply equivalent to producing two molecules of hydrogen and one molecule of oxygen from two molecules of water:

$$2H_2O \longrightarrow 2H_2 + O_2 \tag{12}$$

Since chemical (H_2) energy is being created, a minimum energy must be input to drive the process according to the laws of thermodynamics. In terms of electrical energy, this corresponds to a voltage greater than 1.23V. In reality, the working voltage necessary to sustain water electrolysis is always greater than this. The extra voltage, generally known as the over voltage, represents a waste of energy or loss of efficiency. It has two main causes, one of which is the internal voltage drop loss due to the finite electrical resistance of the electrolyte, or membrane in this case. The second is kinetic in origin, i.e., to do with the overall speed of the process at the electrode surface [20].

A solid catalyst speeds up chemical reactions due to its surface action. As a simple example, two H atoms held loosely on a surface are much more likely to collide and make H_2 gas than if they are dispersed in a liquid with billions of water molecules in-between. This is a spatial or localized concentration effect. The case of O_2 evolution is much more complex. Two water molecules must be broken into their constituent atoms; then the two O atoms must combine. The electro catalyst at the anode is a special catalyst, which facilitates this process by withdrawing electrons from the water such that the H atoms are ejected as protons, which enter the membrane. Water is said to be activated by charge-transfer. The OH or O atoms are very reactive in their free state. However, when fixed at the surface by chemical bonds, they are much more stable. When more water encounters the surface, its protons are ejected in turn and O atoms are

23

accumulated. These are then able to combine easily by surface diffusion just as described for hydrogen. It is said that the surface provides a low-energy pathway, which is intrinsically much faster because the speed of the reaction is related exponentially to the energy difference.

It is easy to visualize that if the cathode and anode surfaces, respectively, attract H or O atoms too strongly, the surfaces will become completely covered with these intermediates and the catalytic process stops. On the other hand, if protons or water are not attracted strongly enough, the process never gets going. Only when there is a moderate strength of binding of reactants and intermediates at the electrode surfaces will the right balance is obtained. This is the key factor in determining if a solid catalyst will work efficiently. It is also obvious that the larger the catalyst surface area available, the more H_2 and O_2 will be produced in a given time, i.e., a higher current will flow in the electrolyzer.

Platinum is long known to be the best catalyst for water electrolysis due to its moderate strength of adsorption of the intermediates of relevance. It has the lowest over-voltage of all metals. However due to its cost, and the preferred operation of the electrolyzer at high current, ingenious ways have been devised to deposit ultra-fine Pt particles either on the electrode support plate, or directly onto the membrane, which is then clamped for good electrical continuity. A current of 1-3 Amperes per square centimeter can be obtained from as little as 3 milligrams of Pt spread over the same area [20].

24

1.8 Literature review

Hydrogen production from water electrolysis using proton exchange membranes (PEM) has been studied to some degree since the development of the first PEM water electrolyzer by the General Electric Company [21]. PEM based electrolyzers benefit over alkaline systems with much higher current densities (1-3 A/cm^2 compared with 0.2 A/cm^2 [22, 23]), no circulating liquid electrolyte, wide range of power loadings, and very rapid power-up/power-down rates. These systems also have the advantage of potentially being utilized as regenerative fuel cells (i.e. the cell works in electrolysis mode when renewable power is available and fuel cell mode when renewable power is not available).

As mentioned above, the cost of PEM based electrolyzers are higher than conventional alkaline systems. A high current density PEM water electrolyzer was investigated as a means of overcoming the disadvantage of the initial cost of these systems [23]. It was shown that the IR drop (i.e., "IR" drop, according to Ohm's Law V=I*R, where R is the equivalent path DC resistance between the source location and the device location and I is the average current the chip draws from the supply) contributed to about 90% of the cell voltage increase over the current density range of 1-5 A/cm^2. Bi-functional electro-catalysts were examined for a regenerative PEM fuel cell [24]. The oxygen electro-catalyst was a 50 wt% Pt black + 50 wt% IrO$_2$, and the hydrogen electro-catalyst a Pt black layer. Another regenerative PEM fuel cell was examined using a mixed Pt black + IrO$_2$ anode electro-catalyst and a Pt-black cathode electro-catalyst at a loading of 8-10 mg/cm^2, and a Nafion 115 membrane [25]. Ruthenium dioxide (RuO$_2$) was examined as the anode electro-catalyst in a solid polymer electrolyte water electrolyzer [26]. Membrane electrode assemblies (MEA's) for water electrolysis were

25

developed using a new plating method in which the noble metal salt precursors were reduced using Na_2BH_4 solution [27].

Coatings of Pt and Ir were used in solid polymer electrolyte water electrolyzers using a chemical reduction process [22]. Further work showed that a Ru-Pt anode initially gave even better cell performance than the Pt-Ir anode, although the cell voltage quickly increased with time due to the dissolution of the Ru within the electrolyte [28].

Millet et al. [29] discussed the design and performance of a PEM water electrolyzer. High cell voltages were contributed to poor electrical connections which introduced a significant ohmic loss. Rasten [30] provided a study of various electro-catalysts for water electrolysis using proton exchange membranes. A solid polymer electrolyzer was developed using IrO_2 as the anode catalyst and Pt black as the cathode catalyst at loadings of 3 mg/cm^2 [31].

Since 1987 Mitsubishi Heavy Industries, Ltd. has been developing solid polymer water electrolyzer technology [32]. A chemical plating technique was used to plate iridium metal onto each side a Nafion membrane. A 50 cm^2 solid polymer electrolyte electrolyzer was developed using a hot press method to adhere the catalyst film to the membrane [33]. Based on the results mentioned above, a 2500 cm^2 solid polymer electrolyte electrolyzer was developed [34]. A high pressure solid polymer electrolyte water electrolyzer was developed with Pt and Ir black serving as the anode catalyst and Pt black as the cathode catalyst [35]. The development of MEA's for a reversible solid polymer fuel cell was examined using Pt, Rh, Ir, and Ir-Ru mixed oxides, as the oxygen evolution electro-catalyst [36]. Millet [37] provided an experimental study for an electrode membrane electrode (EME) cell operated at high current densities. From their

26

experimental work, the electric potential across the cell and membrane alone were computed, since the determination of anodic and cathodic over-voltages usually requires the use of a membrane strip [38, 39]. They also determined if a membrane strip can be used as a reference potential to measure separately each term of the cell voltage.

PEM electrolyzers are particularly suited to small scale and "online" hydrogen production units like at future hydrogen refueling stations. So far, most of the research on PEM electrolyzer cells has focused on experimental studies only. Some results from the simplified models have also been reported recently by Onda et al. [40], Choi et al. [41] and Nie et al. [42]. No numerical analysis has been seen in the published literature yet. The main aim of this thesis is to develop a simple, economical numerical model for an electrolyzer cell that can be compared to the available experimental data and to perform detailed parametric analysis on it.

1.9 Objective of research

The present work is funded by Department of Energy and University of Nevada, Las Vegas. Some of these research objectives are outlined as follows:

- To develop a computational model for the Proton Exchange Membrane (PEM) electrolyzer

- To analyze the performance of this electrolyzer at different temperatures on a two dimensional numerical model

- To study the effects of variation of difference parameters, thickness of the thin permeable membrane and length of the current collector on the cell voltage vs. current density relation (i-V curve) using a two dimensional numerical model

- To compare the simulation results with the available experimental data

27

CHAPTER 2

NUMERICAL MODELING

2.1 Numerical model geometry

A schematic of the PEM electrolyzer cell is shown in Figure 2.1. The formation of the computational geometry from this conceptual design is shown in Figure 2.2 along with dimensional details. It should be noted that only the electrochemical process without sunlight has been modeled in the present thesis. The overall dimensions of this two-dimensional numerical model are 2.5 mm in height and 0.65 mm in width. Selection of these parameters is motivated by the fact that there are measured data available for validating the numerical simulation code. The model comprises of three subdomains (1, 2, and 3). Figure 2.2 describes each subdomain and its notation is explained as follows:

- Subdomain1, SD1, represents the anode

- Subdomain 2, SD2, represents the thin permeable membrane (PEM)

- Subdomain 3, SD3, represents the cathode

The line segments formed by the key points P_2-P_3 and P_8-P_9 represents the current collector of the cell. The line segments formed by the key points P_1-P_2 and P_9-P_{10} correspond to the inlet passages of water. The line segments formed by the key points P_3-P_4 and P_7-P_8 correspond to the outlet passages of oxygen (O_2) and hydrogen (H_2) gases.

28

Water Electrolysis
Reaction:
$2H_2O \rightarrow 4H^+ + 4e^- + O_2$
Occurs at the Anode

Electrons Recombine With
Protons and H_2 Is Produced
At the Cathode:
$4H^+ + 4e^- \rightarrow 2H_2$

Electrocatalysts

PEM

$[H^+]$

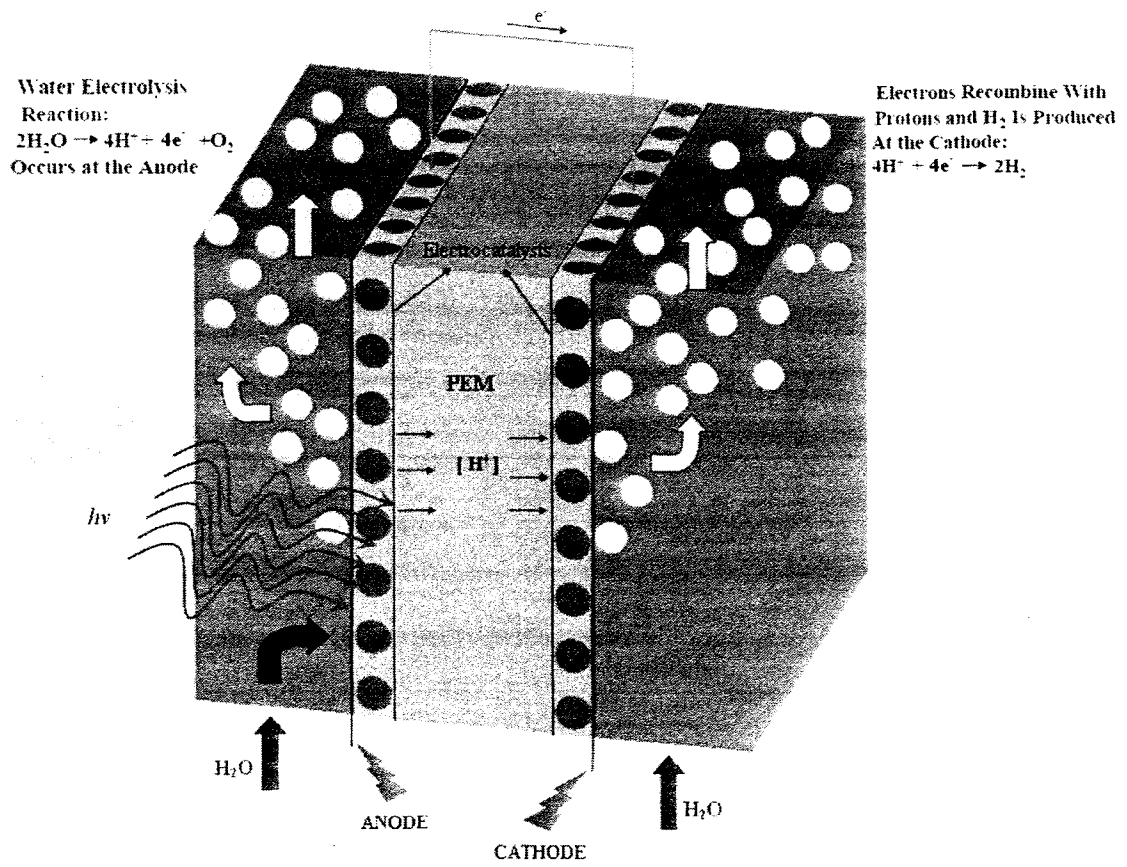hv

H_2O

H_2O

ANODE

CATHODE

Figure 2.1: PEM electrolyzer

29
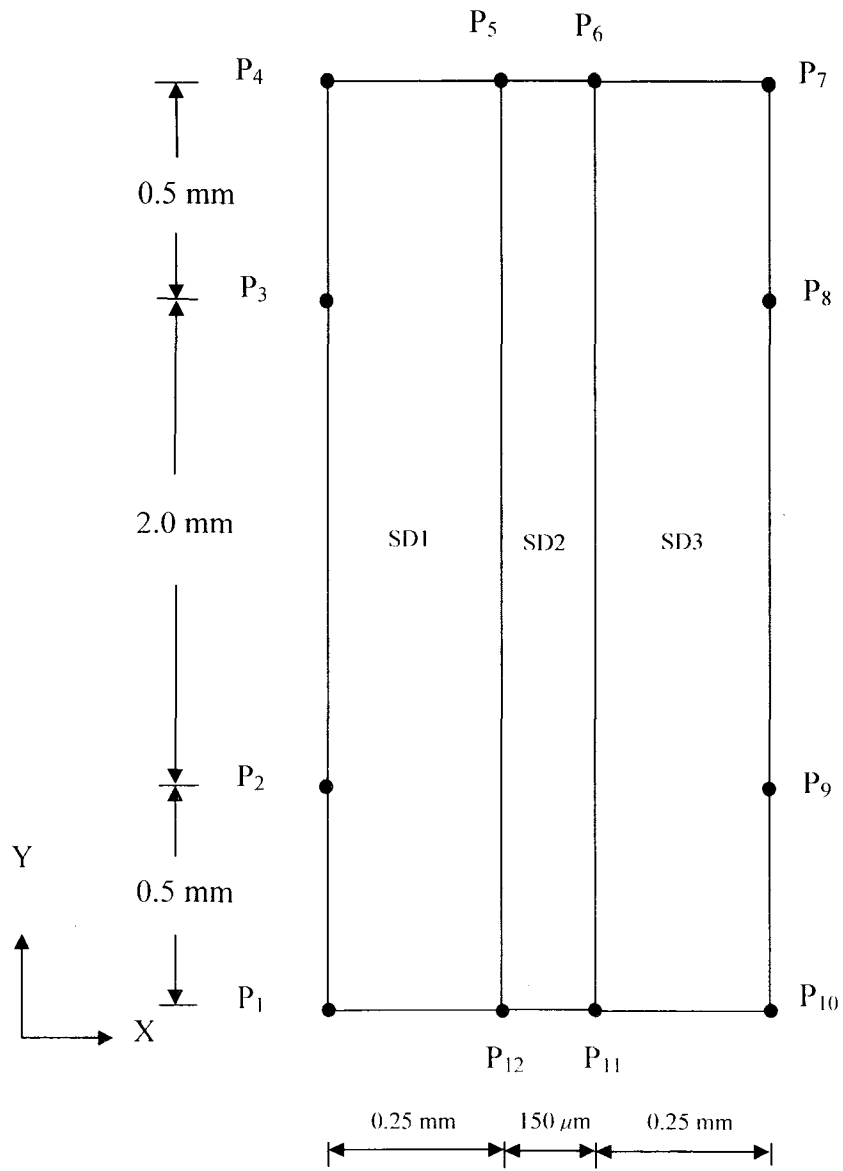
Figure 2.2: Description of numerical model geometry

30

2.2 Numerical model assumptions

A numerical model is developed based on appropriate mass balances, transport, and electrochemical kinetics [43]. The following assumptions are considered in the model:

- In the numerical model, the cell is assumed to operate under steady state condition.

- A two-dimensional, isothermal approximation is used.

- The membrane is considered permeable for the protons and water.

- The cell temperature remains constant.

- The catalyst layers are treated as an infinitely thin surface of reaction.

- The membrane is considered impermeable for the gas phase.

- Water in the membrane is in the liquid phase only, and the water pressure varies linearly in the membrane.

The model uses the Maxwell-Stefan equation to account for the water diffusion in the diffusion layer of both the anode side and the cathode side. Darcy's law is used for the flow of species in the porous electrodes.

2.3 Material properties

The cell consists of two noble metal electrodes deposited on either side of a proton conducting membrane, made up of Nafion[®]. Nafion is a registered trademark of E.I. Du Pont de Nemours, Wilmington, DE, U.S.A., for its per fluoro sulfonic acid materials. Nafion[®] products are chosen as the solid electrolyte because of their intrinsic properties. It has excellent chemical and mechanical stability, high protonic conductivity and gas impermeability. Because of the highly acidic environment produced by

31

sulphonic acid groups at the surfaces of the membrane, acid-resistant noble metals or their oxides must be used for electro-catalysts [37]. The physical parameters of the materials used in the cell are listed in Table 2.1. Selections of these values are motivated by the fact there is experimental data [37] which can be later used to validate the developed numerical model.

The noble metal used for electrodes is platinum (Pt) because it is chemically inert over a wide potential range, so it won't react with the hydroxide ions produced from the splitting of water molecules [20]. Using platinum electrodes, hydrogen gas will be seen to bubble up at the cathode, and oxygen will bubble at the anode. If, however, any other metal is utilized for the anode, the oxygen will react with the anode instead of being released as a gas. For example using iron electrodes in a sodium chloride solution electrolyte, iron oxide will be produced at the anode, which will react to form iron hydroxide. When producing large quantities of hydrogen, this can significantly contaminate the electrolytic cell – which is why iron is not used for commercial electrolysis [44].

Table 2.1: Physical property parameters [41]

Parameter	Value
σ_m, electrical conductivity of membrane (S/m)	14
σ_s, electrical conductivity of anode and cathode (S/m)	570
k_p, permeability of electrode (m^2)	10^{-11}
i_{0a}, anode exchange current density for Pt (A/cm^2)	10^{-12}
i_{0c}, cathode exchange current density for Pt (A/cm^2)	10^{-3}

2.4 Governing equations

2.4.1 Equation for Darcy's law

A simplified form of the momentum equation, Darcy's law for porous media in the water distribution electrodes, states that the gradient of pressure, the viscosity of the fluid, and the structure of porous media determine the velocity vector:

$$\vec{u} = -\frac{k_p}{\mu} \nabla p \qquad (13)$$

where k_p denotes the permeability of the electrode, μ is the viscosity of the water and p is the pressure.

33

2.4.2 Maxwell-Stefan equation

The Maxwell-Stefan equation accounts for the multi-component diffusion in the diffusion layer of the electrode.

$$-c\nabla x_i = \sum_{j=1, i \neq j}^{n} \frac{1}{D_{ij}}(x_j \vec{N}_i - x_i \vec{N}_j) \tag{14}$$

where c is the concentration of the mixture, D_{ij} is the ordinary or binary diffusion coefficient of species i in j, x_i is the mole fraction of species i, and $\vec{N}_i$ is the diffusion flux of species i. The binary diffusivities, D_{ij}^0, can be obtained experimentally. Its values at reference pressure, p_0 (i.e., atmospheric pressure p_{atm} in the present study) and reference temperature, T_0, is shown in Table 2.2 according to [45]:

$$D_{ij} = D_{ij}^o (T_o, p_o) \frac{p_o}{p} \left(\frac{T}{T_o} \right)^{1.5} \tag{15}$$

Table 2.2: Binary diffusivities at 1 atm [45]

Gas pair	Reference temperature, T_0 (K)	Binary diffusivity, $D_{ij}(T_0, p_0)$ (m^{2}s^{-1})
$D_{H_2-H_2O}^0$	307.1	9.15×10^{-5}
$D_{O_2-H_2O}^0$	308.1	2.82×10^{-5}

34

2.4.3 Equation for species balance

The species balance equations in the porous electrodes are described with the following equation:

$$\nabla \cdot \left(-\rho \omega_i \sum_j \left(D_{ij} \nabla x_j + (x_j - \omega_j) \frac{\nabla p}{p} \right) + \rho \omega_i u \right) = 0 \tag{16}$$

$$x_j = \frac{\omega_j}{M_j} \cdot M_{Total} \tag{17}$$

where the mole fraction, x, is calculated using the Eq.17 with x_i expressed in terms of the mass fractions, ω, and molecular weights, M. For the anode, i represents two species, (O_2, H_2O) and for the cathode, it represents two species, (H_2, H_2O). ρ is the mixture density, a function of the mole fractions and molecular weights, according to the equation:

$$\rho = \frac{M_{Total}}{RT} \cdot p \tag{18}$$

$$M_{Total} = \frac{1}{\sum_k \frac{\omega_k}{M_k}} \tag{19}$$

$$\sum_{k=1}^{n} \omega_k = 1 \tag{20}$$

where p is the pressure, T is the cell temperature and R is universal gas constant (8.314 J/(mol.K)).

2.4.4 Equation for charge balance in electrode

The charge balance in the water distribution electrodes is solved using the following continuity relationship:

$$-\nabla \cdot (\sigma_s \nabla \phi_s) = 0 \tag{21}$$

35

where σ_s is the effective conductivity and ϕ_s is the electric potential in the electrode.

2.4.5 Equation for charge balance in membrane

The membrane is assumed to be impermeable to the gases of oxygen and hydrogen. Therefore, the membrane is composed of only water and protons. Each of these species must obey the principle of mass conservation with the balance of charge in the membrane represented by the continuity relationship:

$$- \nabla.(\sigma_m \nabla \phi_m) = 0 \tag{22}$$

where σ_m is the conductivity of the membrane and ϕ_m is the membrane potential.

2.4.6 Butler-Volmer equation

The Butler-Volmer equation describes the relationship between the current density and the activation losses at the catalyst surface [46].

$$i_a = i_{0a} \left[\exp\left(\alpha_a \frac{nF}{RT} \eta_a \right) - \exp\left((1-\alpha_a) \frac{nF}{RT} \eta_a \right) \right] \tag{23}$$

$$i_c = i_{0c} \left[\exp\left(\alpha_c \frac{nF}{RT} \eta_c \right) - \exp\left((1-\alpha_c) \frac{nF}{RT} \eta_c \right) \right] \tag{24}$$

where i_a and i_c are anode and cathode current densities, η_a and η_c are the activation over potential or the electrode losses for anode and cathode, i_{0a} and i_{0c} are the exchange current densities, α_a and α_c are the anodic and cathodic charge transfer coefficients,

respectively, and n is the number of electrons participating in the electrochemical reaction.

2.4.7 Equation for electrode over-potential

The over potential for the cathodic reaction represented by Eq.4 is defined as:

$$\eta = \phi_s - \phi_m \tag{25}$$

Similarly, the over-potential for the anodic reaction represented by Eq.5 is the difference between the electrode and the membrane potentials and the open circuit potential. It can be defined as:

$$\eta = \phi_s - \phi_m - V_{OC} \tag{26}$$

where ϕ_s and ϕ_m are the anode and membrane potentials at the catalyst surface, and V_{OC} is the Nernst potential for the overall reaction represented by Eq.6 and is empirically given as [47]:

$$V_{OC} = 1.229 - 0.9 \times 10^{-3}(T - 298) + 2.3\frac{RT}{4F}\log\left(p_{H_2}^2 \, p_{O_2}^2\right) \tag{27}$$

where F is Faraday's constant (96485.3 C/mol) and p_{H_2}, p_{O_2} are the pressures of hydrogen and oxygen gases respectively.

This can be reduced to [48]:

$$V_{OC} = 0.2329 + 0.0025 \times T \tag{28}$$

2.5 Boundary Conditions

2.5.1 Current density boundary condition for anode catalyst reactive layer

The boundary conditions for the current density at the catalyst interface between the anode and the membrane are given by:

37

$$\vec{n}.\left(-\sigma_s \nabla \phi_s\right) = i_a \tag{29}$$

$$\vec{n}.\left(-\sigma_m \nabla \phi_m\right) = -i_a \tag{30}$$

where $\vec{n}$ is the unit vector in the normal direction away from the domain.

2.5.2 Current density boundary condition for cathode catalyst reactive layer

Similarly, for the catalyst interface between the cathode and the membrane, the boundary conditions for the current density are specified by:

$$\vec{n}.\left(-\sigma_s \nabla \phi_s\right) = i_c \tag{31}$$

$$\vec{n}.\left(-\sigma_m \nabla \phi_m\right) = -i_c \tag{32}$$

where $\vec{n}$ is the unit vector in the normal direction away from the domain.

The potential at the current collector on the cathode side is defined as 0 V, and the potential at the current collector on the anode side is specified as V_{cell}. The insulated boundary condition is employed for the remaining boundaries.

2.5.3 Mass flux boundary condition for anode catalyst reactive layer

The mass flux of oxygen and water at the anode catalyst reactive boundary is calculated by the boundary condition:

$$\vec{n}.\left(-\rho\omega_{O_2}\left(D_{O_2-H_2O}\nabla x_{O_2}+\left(x_{O_2}-\omega_{O_2}\right)\frac{\nabla p}{p}\right)+\rho\omega_{O_2}\vec{u}\right) = \frac{i_a}{4F}M_{O_2} \tag{33}$$

$$\vec{n}.\left(-\rho\omega_{H_2O}\left(D_{O_2-H_2O}\nabla x_{H_2O}+\left(x_{H_2O}-\omega_{H_2O}\right)\frac{\nabla p}{p}\right)+\rho\omega_{H_2O}\vec{u}\right) = \frac{-i_a}{2F}M_{H_2O} \tag{34}$$

where $\vec{n}$ is the unit vector in the normal direction away from the domain.

38

2.5.4 Mass flux boundary condition for cathode catalyst reactive layer

Similarly, the mass fraction of hydrogen at the cathode catalyst reactive boundary is calculated by the boundary condition:

$$\bar{n}.\left(-\rho\omega_{H_2}\left(D_{H_2-H_2O}\nabla x_{H_2}+\left(x_{H_2}-\omega_{H_2}\right)\frac{\nabla p}{p}\right)+\rho\omega_{H_2}\bar{u}\right)=-\frac{i_c}{2F}M_{H_2} \qquad (35)$$

where $\bar{n}$ is the unit vector in the normal direction away from the domain.

The mass fraction of water on the cathode side is calculated by the boundary condition:

$$\omega_{H_2O}=1-\omega_{H_2} \qquad (36)$$

The boundary conditions for each species at the inlet of the water diffusion electrodes are specified as constants and their values are tabulated in Table 2.3. At the outlet passages convective flux boundary conditions are applied. The insulated boundary condition is applied for other remaining boundaries.

2.5.5 Darcy's Law boundary condition

The pressures at the inlet passages are represented by $pref$, which is the atmospheric pressure. At the outlet passages, p_a and p_c pressures are applied on anode and cathode sides respectively whose values are tabulated in Table 2.3.

39

Table 2.3: Operating condition parameters

Parameter	Value
p_a, anode side pressure (Pa) [49]	111485
p_c, cathode side pressure (Pa) [49]	111485
$x^0_{H_2O,a}$, anode feed water mole fraction	1.0
$x^0_{H_2O,c}$, cathode feed water mole fraction	1.0

All these governing equations and their respective boundary conditions are mentioned in Figure 2.3.
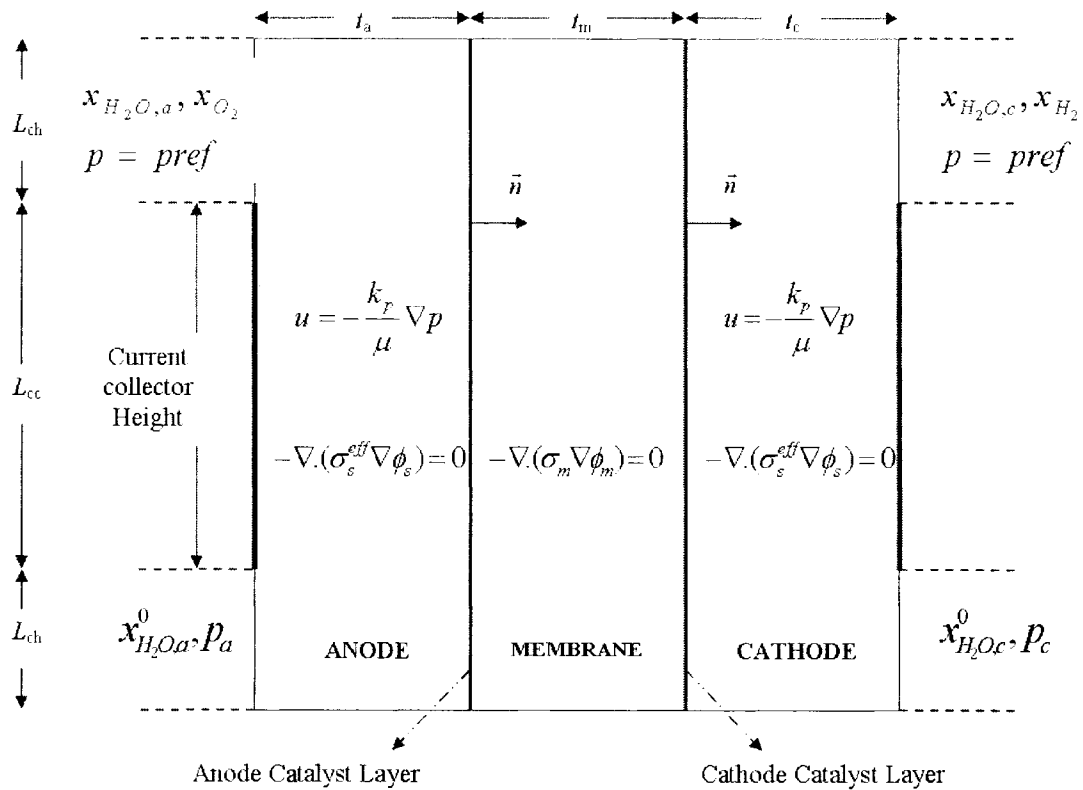

Figure 2.3: Computational domain and governing equations

2.6 Model mesh

All the equations, Eq.13 through 36 were discretized using finite element method and solved using a general purpose multi-physics package, COMSOL (Femlab) 3.2 [52].

For a 2D geometry, we can choose to generate an unstructured mesh consisting of triangular elements or a mapped mesh consisting of quadrilateral elements. The quadrilateral elements are selected to map the computational domain because all the sub-domains are fairly regular in shape.

Uniform grid with quadrilateral elements was employed with more elements near the electrode surfaces, where concentration gradients are expected to be high. A steady Direct UMFPACK linear system solver was used.

Several numerical simulations were performed in order to ensure that the obtained solutions were independent of the grid size. Several grids were selected for the purpose of grid-independence test: 225 (elements) by 256 (nodes), 900 by 961, 3600 by 3721, 8100 by 8281, 14400 by 14641, 22500 by 22801, and 32400 by 32761. The finer mesh of 14400 by 14641 results in less than 5% difference in the predicted current density compared with the mesh size of 32400 by 32761. Therefore, from Figure 2.5, the mesh with 14400 elements and 14641 nodes has been selected for the present simulations. The current density at (0.65mm, 2mm) is chosen as the observation point and its values are shown in Figure 2.6 for the selected grids.

41
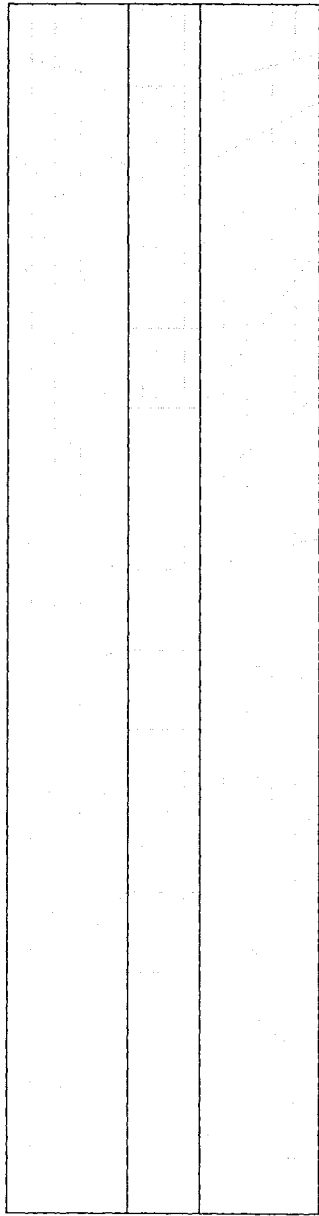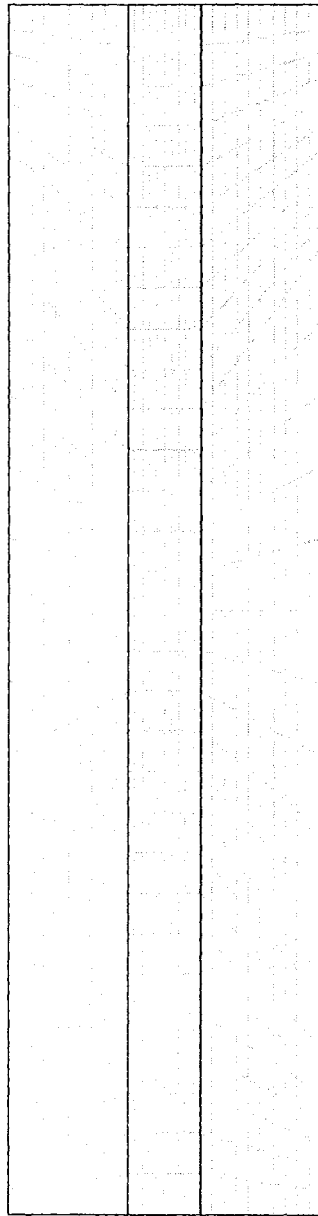
(a) 225 elements   (b) 900 elements   (c) 3600 elements

42
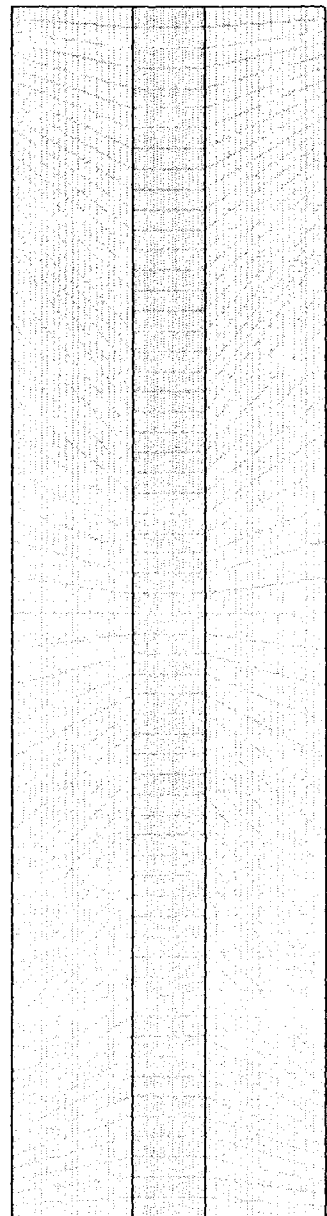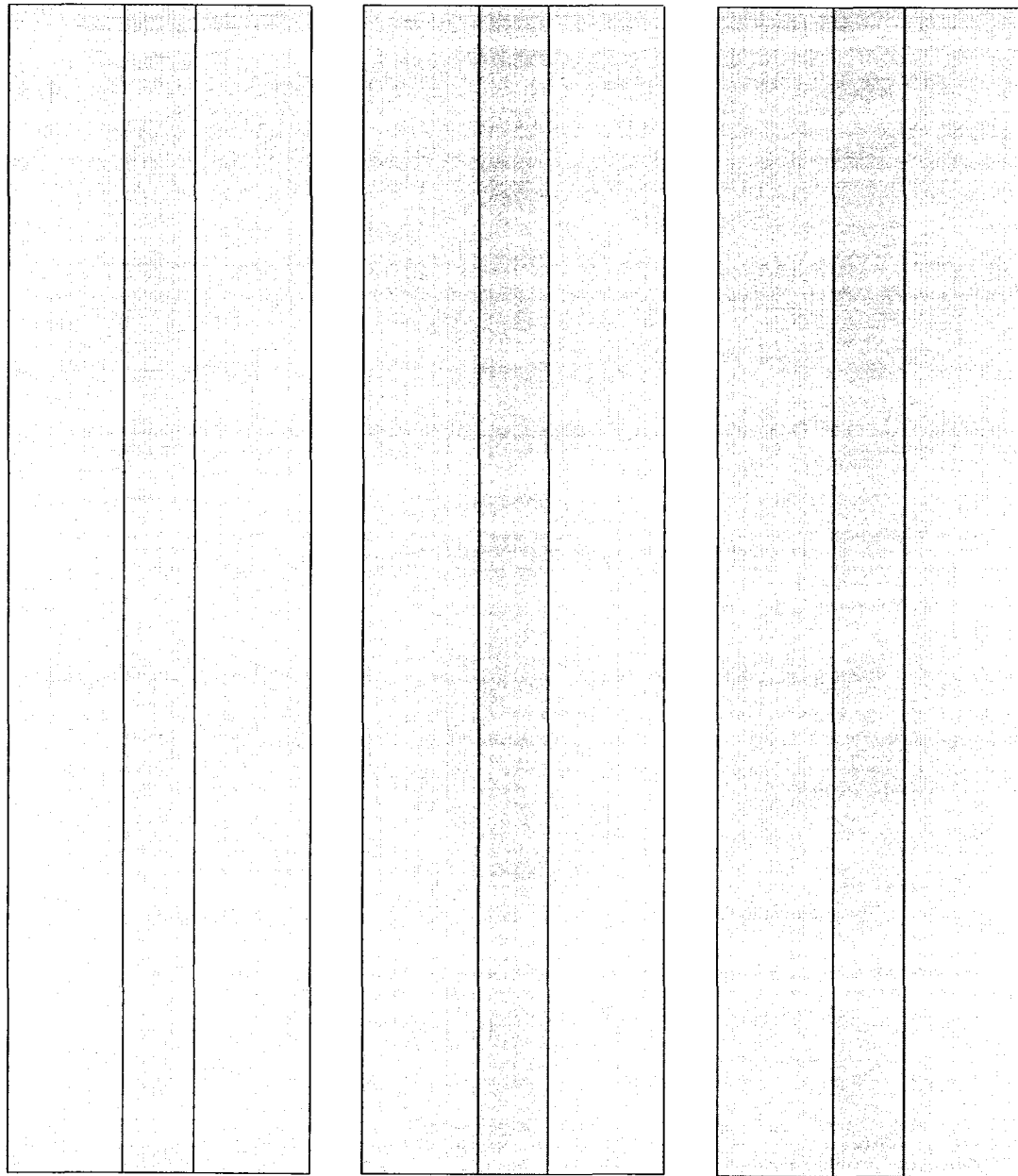
(d) 8100 elements   (e) 14400 elements   (f) 22500 elements

Figure 2.4: Different mesh density plots of the cell

43
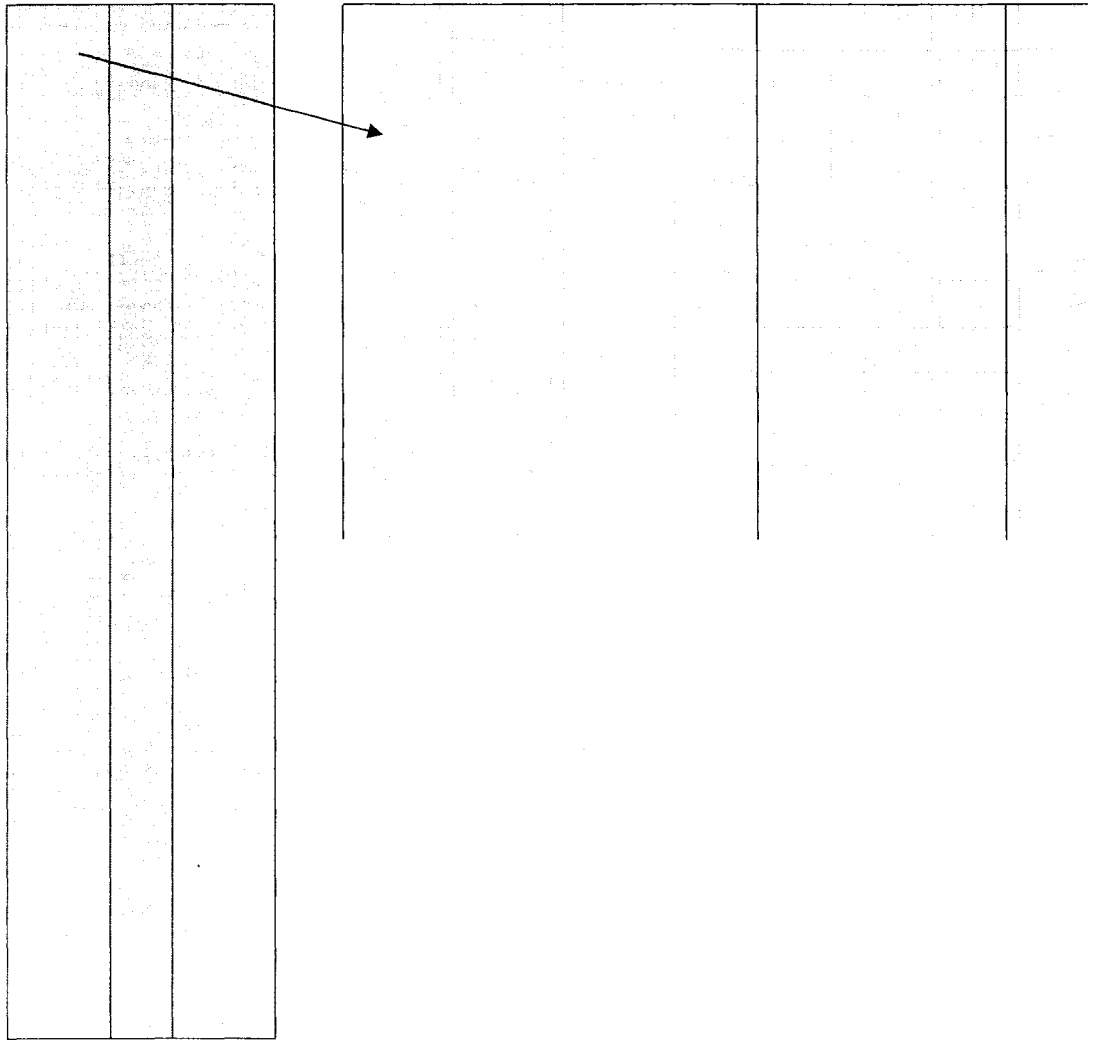
Figure 2.5: Mesh with 14400 elements and 14641 nodes is chosen for numerical simulations

44
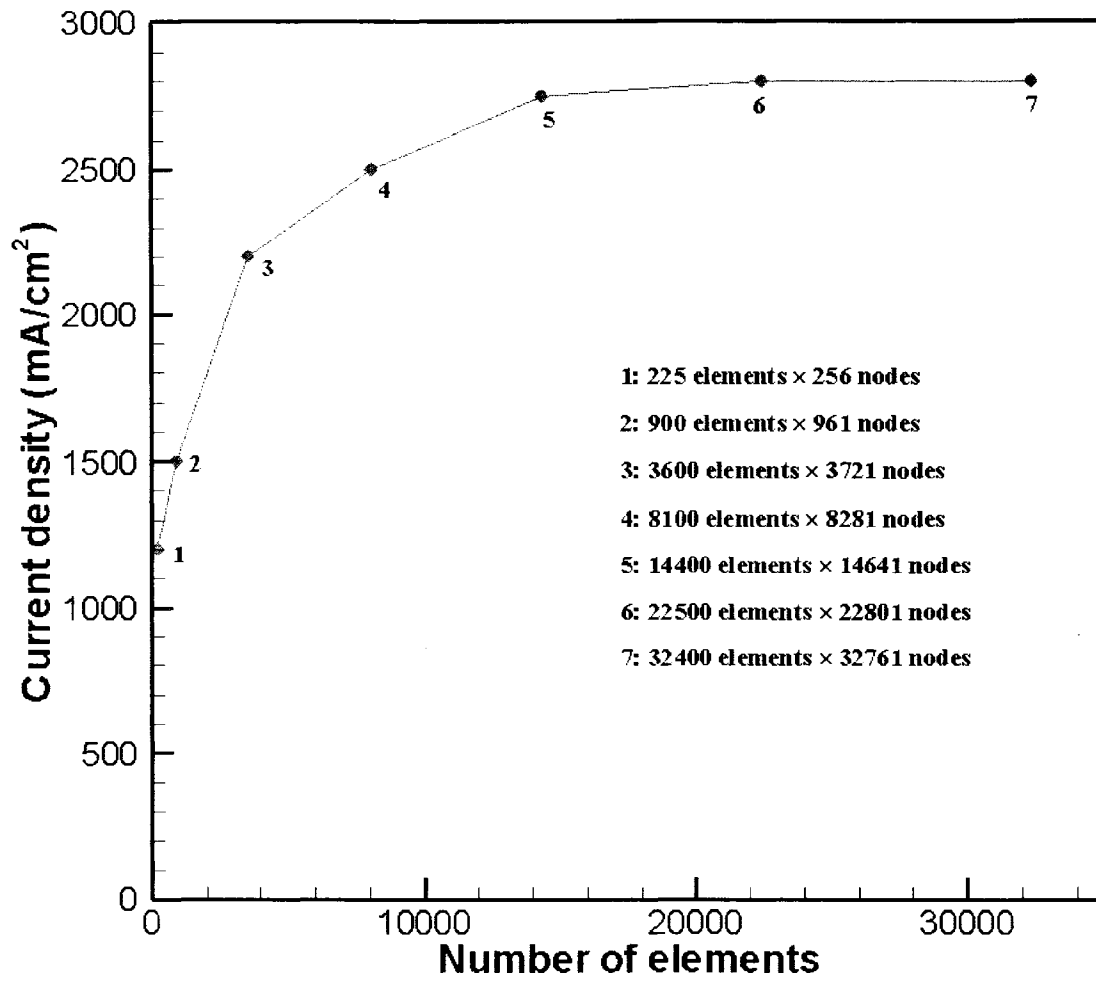
Figure 2.6: Grid independence test

The plot shows Current density (mA/cm^2) on the y-axis (0 to 3000) versus Number of elements on the x-axis (0 to 30000). Legend:

1: 225 elements × 256 nodes
2: 900 elements × 961 nodes
3: 3600 elements × 3721 nodes
4: 8100 elements × 8281 nodes
5: 14400 elements × 14641 nodes
6: 22500 elements × 22801 nodes
7: 32400 elements × 32761 nodes

45

CHAPTER 3

RESULTS AND DISCUSSIONS

3.1 Numerical model validation

Numerical simulations were performed for the electrolyzer cell with geometric parameters tabulated in Table 3.1. Selections of all these geometric parameters are motivated by the fact that there are measured data [37] available for a single cell operated at different cell potentials for the purpose of validating the numerical model developed in the present work. Figure 3.1 shows the current density plot from the numerical model simulation at a cell temperature of 80°C, cell potential of 2.009 V, and membrane thickness of 180 μm.

Figure 3.2 shows the comparison of the i-V curve between the computed results and the available experimental data. Numerical curves show good agreement with the measured data for the current-voltage plot $(i$-V plot). Typical modeling results of cell includes i-V plot at different cell temperatures are shown in Figure 3.3.

This section also focuses on the application of the water transport model to two-dimensional electrolyzer cell. This allows for the investigation of water transport phenomena and its effect on the performance of the cell. A series of two-dimensional simulations are performed. The focus of these simulations is on the prediction of

46

hydrogen, oxygen and water content profiles within the cell as well as the resulting current density distribution.

In the present study, the anode side is assumed to consist of oxygen and water in its aqueous form, while the cathode side consists of hydrogen and aqueous water.

Table 3.1: Geometric parameters

Parameter	Value
L_{ch}, Water channel length (m)	0.5×10^{-3}
L_{cc}, Current collector length (m)	2.0×10^{-3}
t_a and t_c, anode and cathode water distribution electrode thickness (m)	0.25×10^{-3}

In Figures 3.4 and 3.5, the distributions of molar fraction of water and oxygen at the anode side in the cell are shown. Due to the oxidation, the oxygen concentration is greatly increased in the anode water channel.
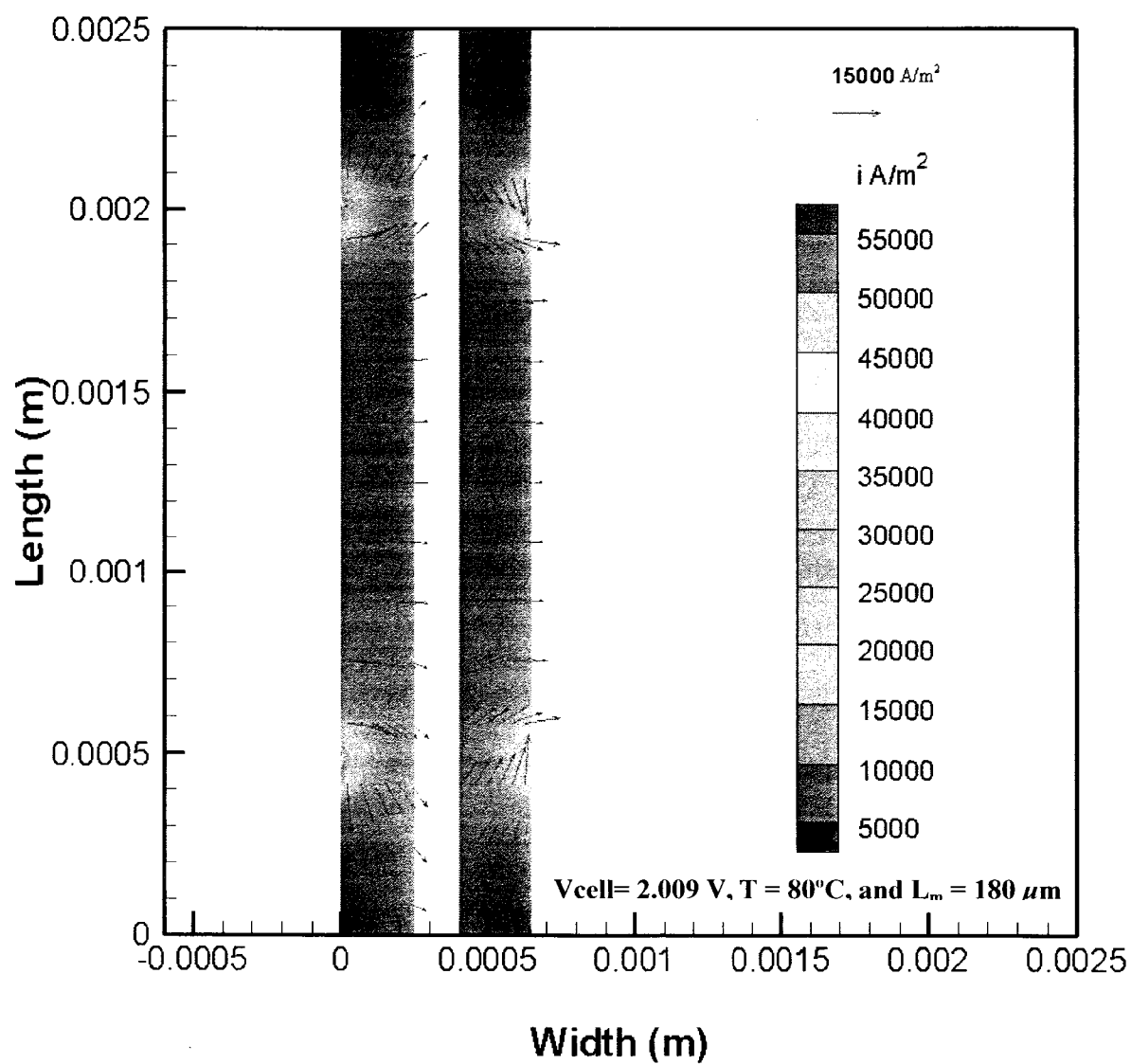
47

Figure 3.1: Distribution of current density across electrodes along with its flow direction
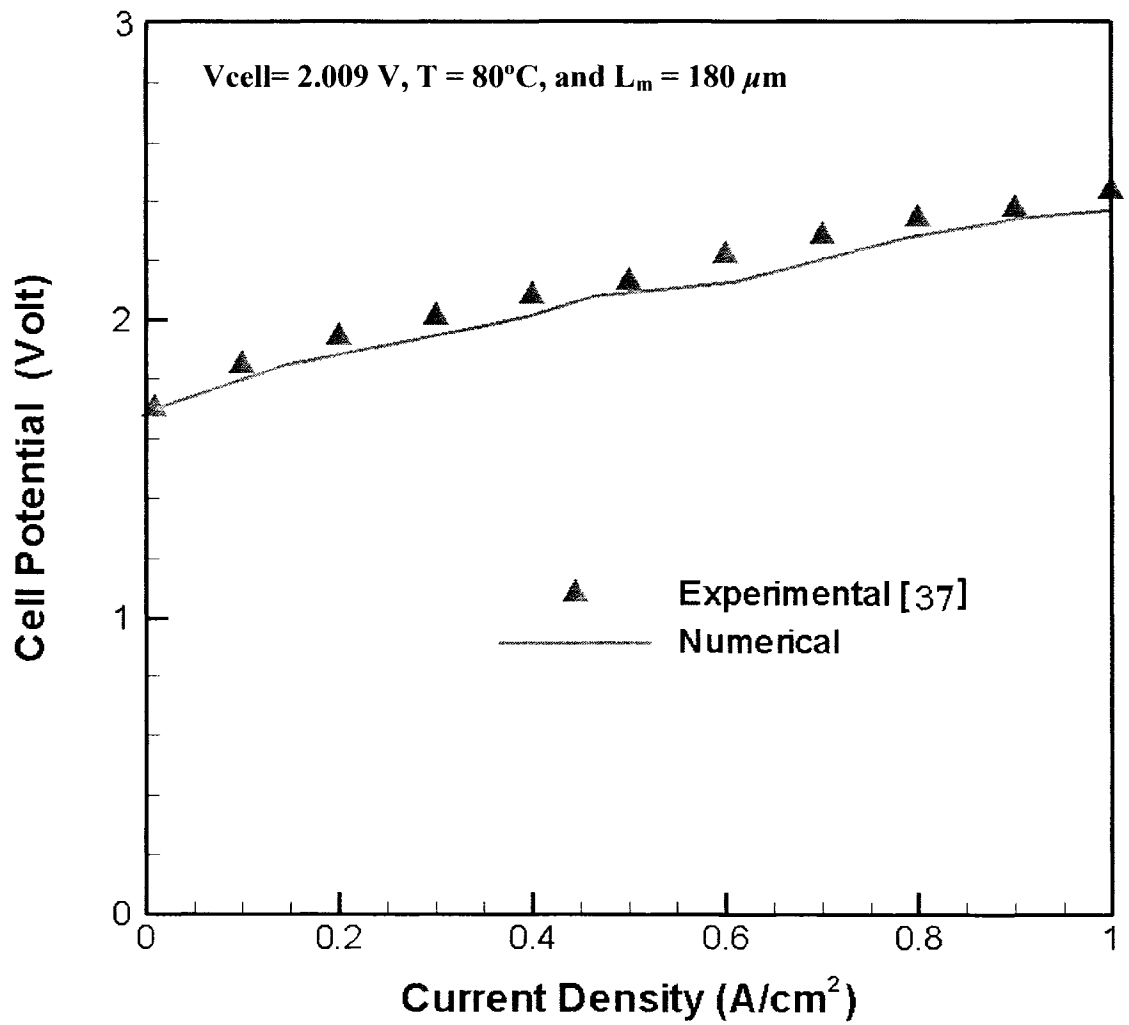
48

Figure 3.2: Comparison of numerically computed cell potential vs. current density with the measurement data [37]
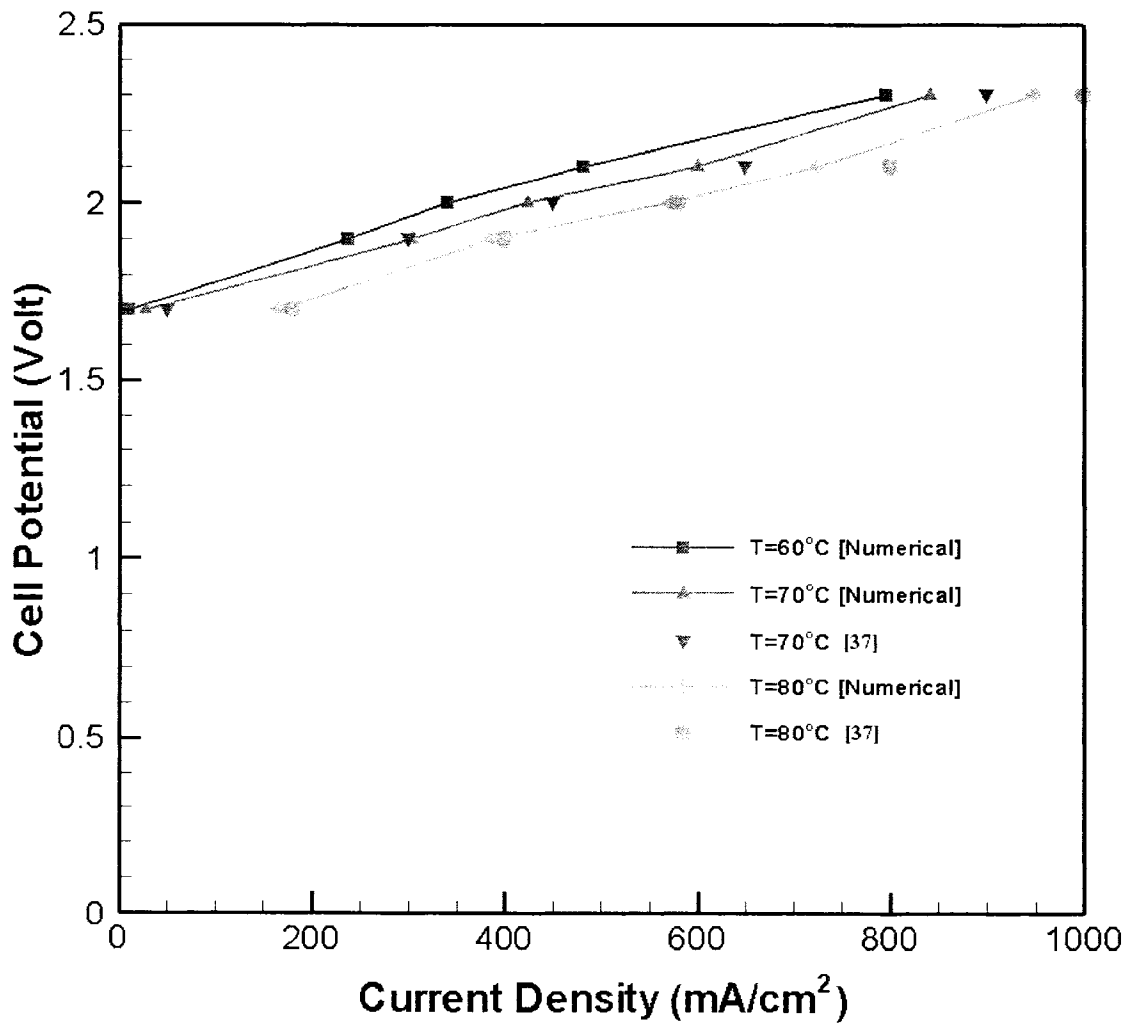
49

Figure 3.3: Comparison of computed current density at various cell temperatures with the measurement data

50

3.2 Numerical results

Numerical simulations for hydrogen production via PEM water electrolysis cell are performed and the simulated results are obtained for a cell potential of 2.009 Volts.

3.2.1 Water mass fraction distribution

Figure 3.4 shows the distribution of water mass fraction in the anode water channel. The mass fraction of water at the inlet passages of the anode and cathode sides is of unit value. With electrochemical reactions, the water molecules are consumed by the splitting reaction. The different colors in the plot represent different magnitudes of the mass fraction of water.

The mass fraction of water at the anode side is obtained by integrating along the boundary of its outlet passage and its average value is 0.497. This reduction in mass fraction corresponds to the amount of water being consumed during the water splitting reaction at the anode side. The water mass fraction at the cathode side does not involve in water splitting reaction instead it is used for hydrating the thin permeable membrane otherwise its conductivity deteriorates.

51
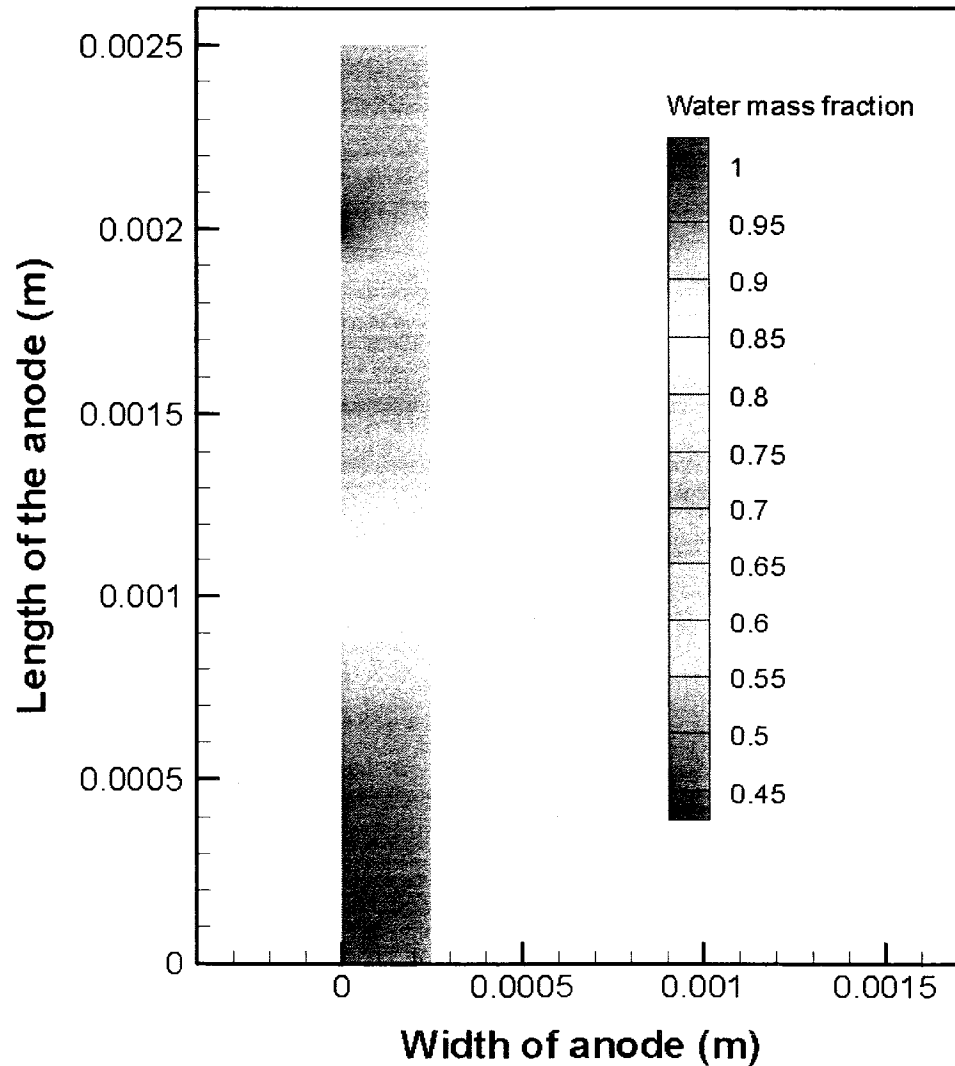
Figure 3.4: Distribution of water mass fraction on the anode

3.2.2 Oxygen mass fraction distribution

Figure 3.5 shows the distribution of oxygen mass fraction across the anode of the cell. The mass fraction of oxygen increases along the anode because of the splitting of water molecules into hydrogen protons (H^+) and oxide ions (O^{2-}) and corresponding oxidation of these oxide ions into oxygen (O_2) gas at the anode. The mass fraction of oxygen is high at the upper corner of the current collector and its magnitude at that

52

location is 0.584, while it is low at the lower corner because initially there is zero oxygen content in the feed water and then later on oxygen is formed.

Figure 3.5: Distribution of oxygen mass fraction on the anode side

53

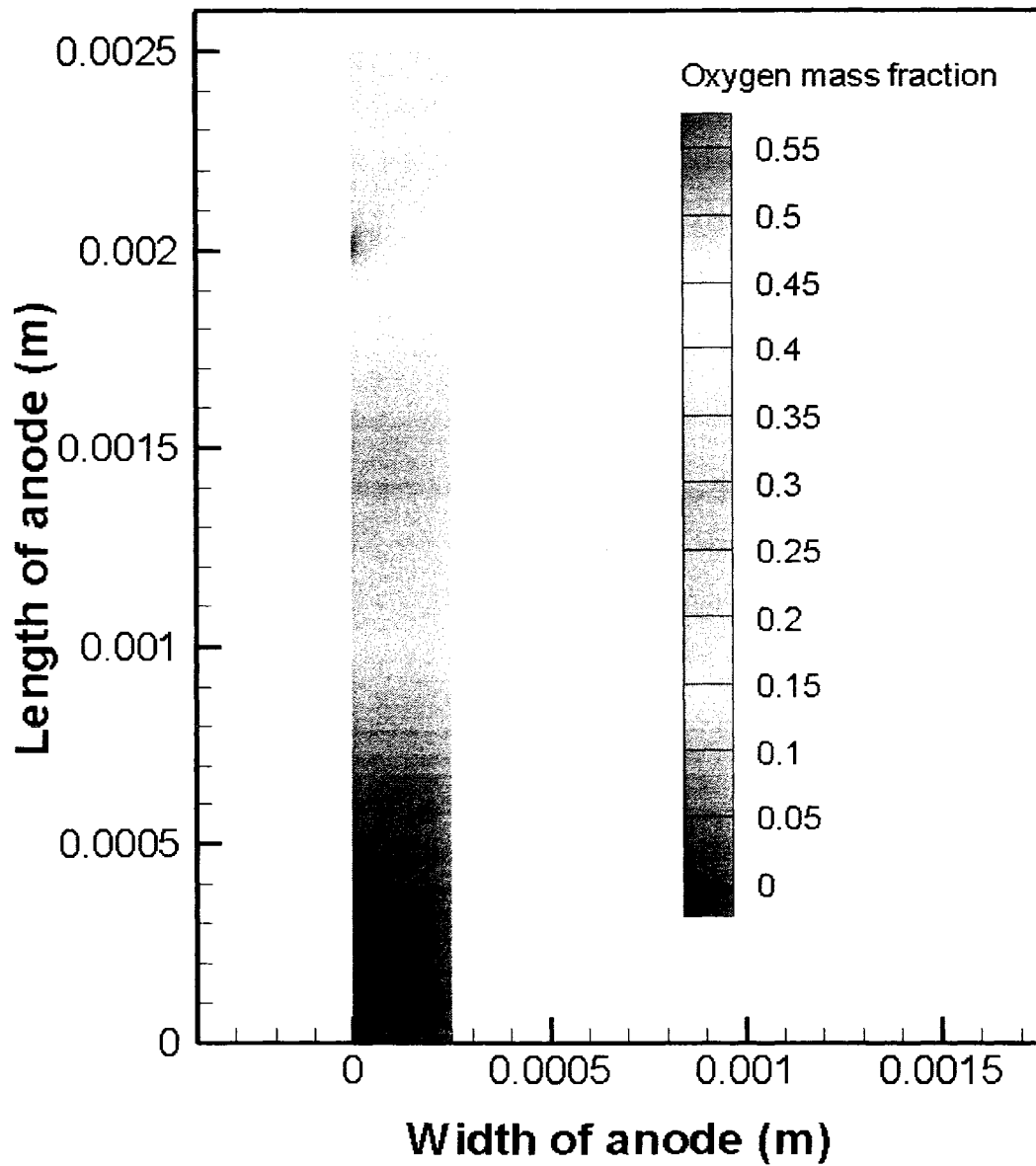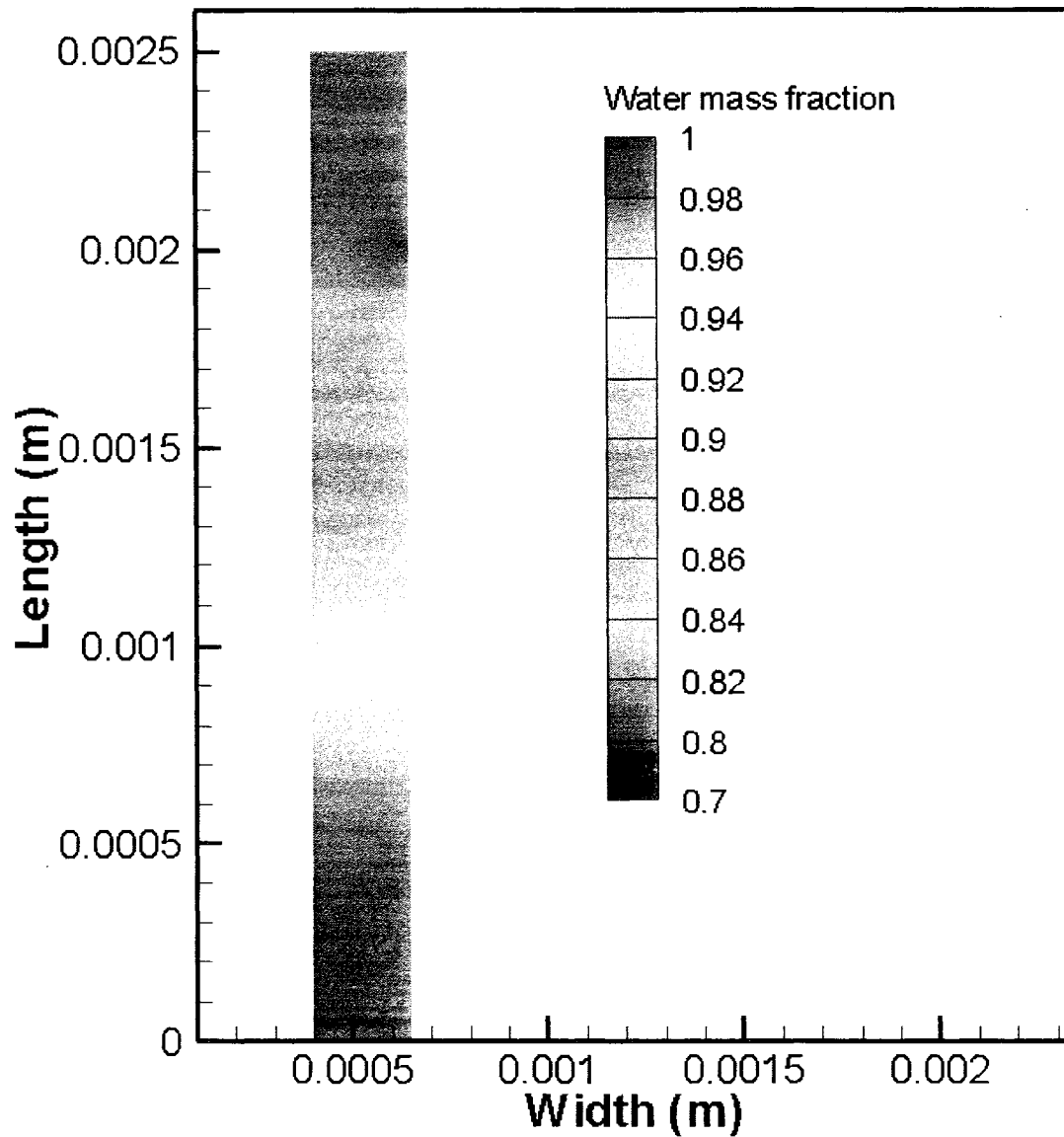Figure 3.6: Distribution of water mass fraction on the cathode side along with the

direction of flow of current density

3.2.3 Hydrogen mass fraction distribution

Figure 3.7 shows the distribution of hydrogen mass fraction across the cathode of

the cell. As the mass fraction of aqueous feed water decreases, the mass fraction of

54

hydrogen increases because of the reduction reaction of hydrogen protons (H^+) into hydrogen (H_2) gas. On the cathode side, the mass fraction of hydrogen gas is high at the upper corner of the current collector and its magnitude at that location is 0.22 approximately, while it is low at the lower corner of the current collector. From the figure, there is zero mass fraction of hydrogen at the inlet passage of the feed water and an average value of mass fraction along the boundary of the outlet passage is 0.185.

All the above mentioned numerical results conclude that the mass fraction of oxygen at the anode side increases more greatly than the mass fraction of hydrogen at the cathode side because each oxygen molecule weighs nearly sixteen times that of a single hydrogen molecule. But when we convert these mass fractions into mole fractions using Eq.14, we indeed obtain 0.8125 moles of hydrogen at the cathode which is more than 0.1875 moles of oxygen obtained at the anode, same as that in the actual water splitting reaction.

3.2.4 Proton exchange membrane

Figure 3.8 shows the distribution of cell potential across the thin permeable membrane of the cell. The plot also depicts the direction of flow of total current density across the membrane. The current density is relatively uniform in the membrane. There is a decrease in the electric potential across the membrane when viewed from the anode side to the cathode side.

55
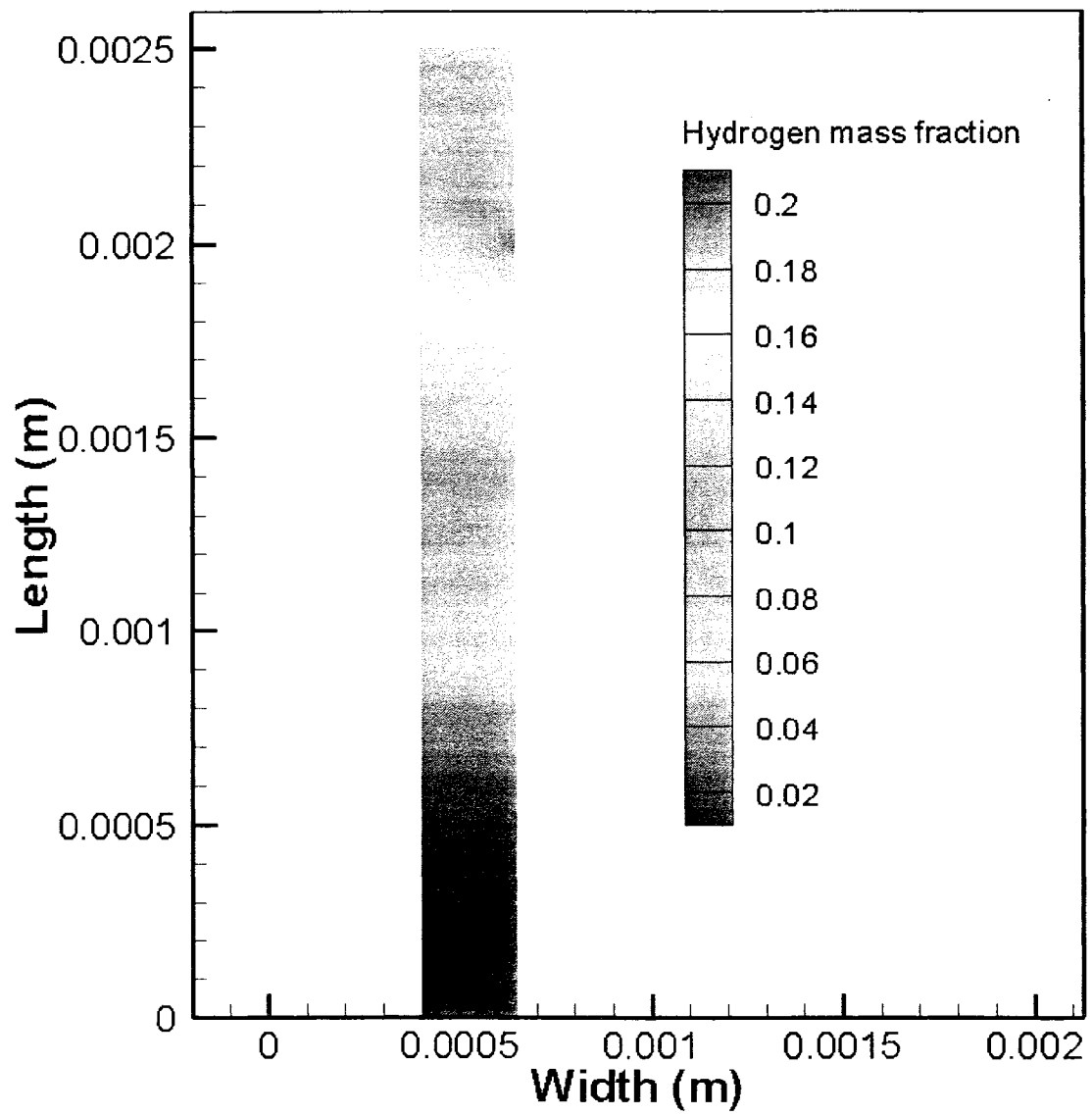
Figure 3.7: Distribution of hydrogen mass fraction on the cathode side

56

0.0025

0.002

Length (m) 0.0015

0.001

0.0005

0

0   0.0005   0.001   0.0015   0.002

Width (m)

5500 A/m²

ϕ_m volt

- 0.21
- 0.215
- 0.22
- 0.225
- 0.23
- 0.235
- 0.24
- 0.245
- 0.25
- 0.255
- 0.26
- 0.265
- 0.27
- 0.275
- 0.28
- 0.285
- 0.29
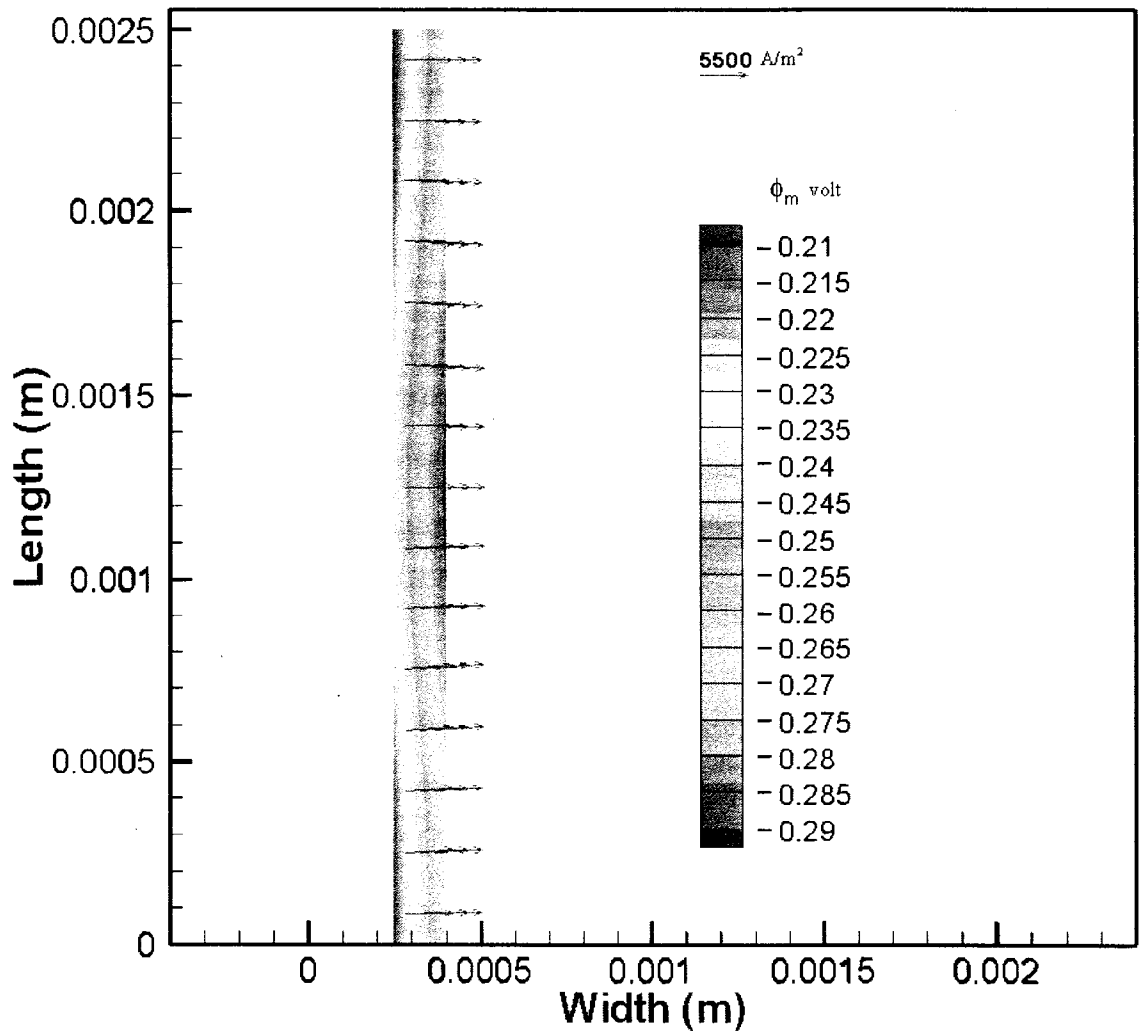
Figure 3.8: Distribution of electric potential across the membrane along with the direction

of flow of current density

3.2.5 Efficiency

Electrolyzers are not constrained by the maximum Carnot cycle efficiency as combustion engines are, because they do not operate with a thermal cycle. The efficiency is a measure of what fraction of electrical energy used is actually contained within the hydrogen. Many researchers have expressed energy efficiency as a percentage calculated

57

from the energy contained in the resulting hydrogen divided by the energy it takes to make that hydrogen [50]. This is a more directly comparable unit of electrolysis efficiency, since it is independent of assumptions regarding electricity and delivery costs. The efficiency of an electrolyzer is very dependent on the current through the cell and it varies widely. This efficiency is based on the high heating value of hydrogen. The energy efficiency of an electrolyzer cell is formulated as [50],

$$\eta_{energy} = \frac{E_{hydrogen}}{E_{electric}} = \frac{V_{H_2} \cdot H_u}{V \cdot I \cdot t} \tag{32}$$

where H_u is the gross calorific value of hydrogen $= 12.745 \times 10^6$ J/m^3 (also called as 'upper heating value'); V_{H_2} is the volume of hydrogen produced in m^3; V is the cell voltage in volts; I is the current in amperes and t is time in seconds.

Numerically solving the model with a cell potential of 2.009 V, the current value obtained across the cell is 0.3938 amperes. The rate of hydrogen volume produced along the outlet passage is calculated by converting the average value of hydrogen mass fraction at the outlet into number of moles of hydrogen and since single mole contains 22.4 liters of gas, it can be further converted into cubic meters and finally into rate by dividing per second. Hence its value is around 7.84×10^{-6} m^3/sec. Therefore, substituting all these values into Eq. 32, the energy efficiency of the electrolyzer model is obtained as 54% approximately. This means that 54% of the electrical energy with which we operate the electrolyzer is stored in the hydrogen gas.

58

3.2.6 Parametric study

Parametric studies have been performed to study the performance and transport mechanisms of PEM electrolyzer cells. These studies include the effect of the thin permeable membrane thickness on the performance of PEM electrolyzer cell, the effect of the length of current collectors on the performance of PEM electrolyzer cell and the effects of operating parameter on the hydrogen production rate of the PEM electrolyzer cell.

a) The effects of temperature on cell potential versus current density curve of cell

In the experimental studies, the effect of operating parameters on the PEM electrolyzer cell performance i.e., the effects of the cell temperature is considered. Based on the numerical results, at constant cell potential, with an increase in the temperature of the cell, there is corresponding increase in the current density across the cell. Figure 3.3 describes this effect in detail.

b) The effect of the thin permeable membrane (PEM) on the performance of cell

As the thickness of the thin permeable membrane increases, the current density across the cell decreases. This can be seen in Figure 3.9. As the current density decreases, the mass fraction of hydrogen decreases and so there is reduction in the production rate of hydrogen correspondingly. Hence, the membrane should be as thin as possible in order to allow maximum current density flow across the entire cell.

c) The effect of the length of current collectors on the performance of the cell

The electric potential is applied to the current collectors of the cell. From Figure 3.10, it can be found that as the lengths of these collectors increase, the current density across the cell increases because of the increase in the collector area of the cell

59

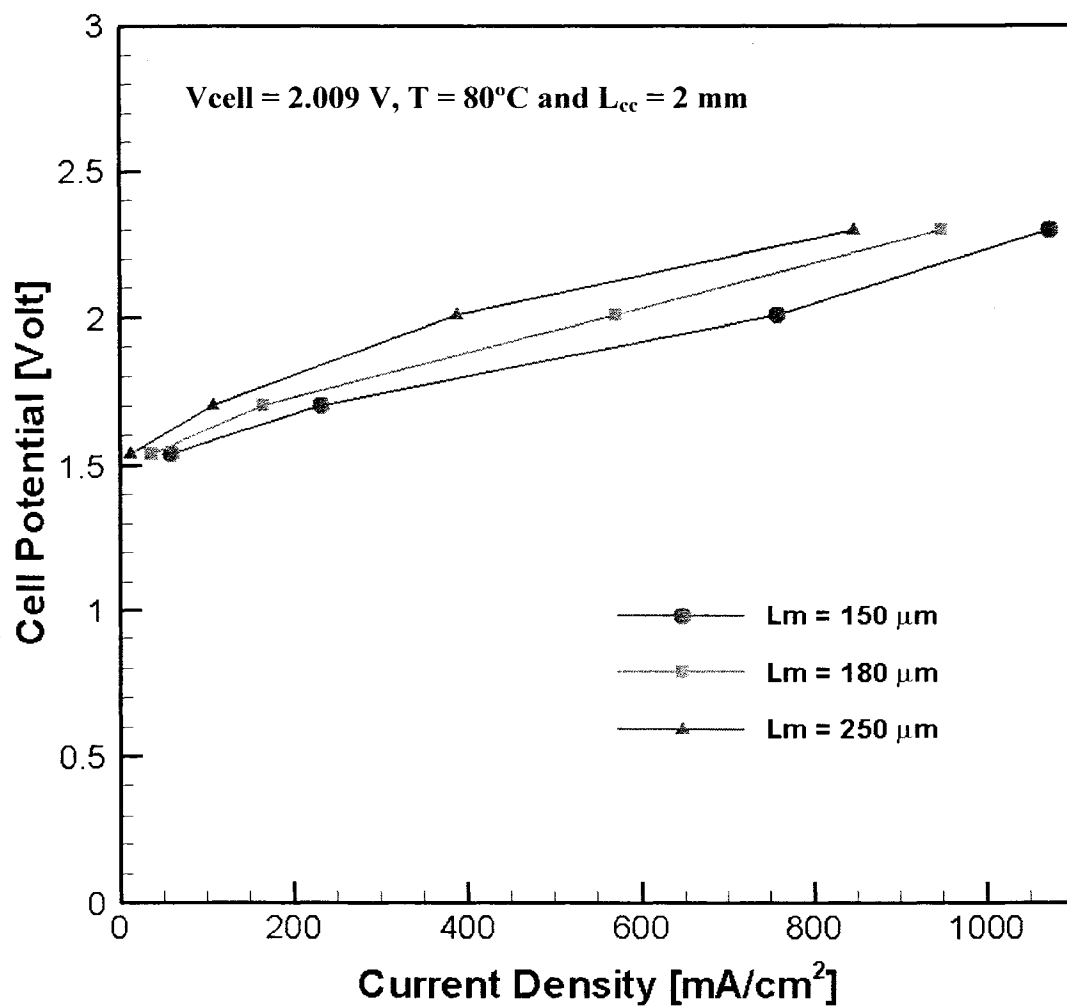Figure 3.9: Influence of various membrane thickness on the cell potential vs. Current
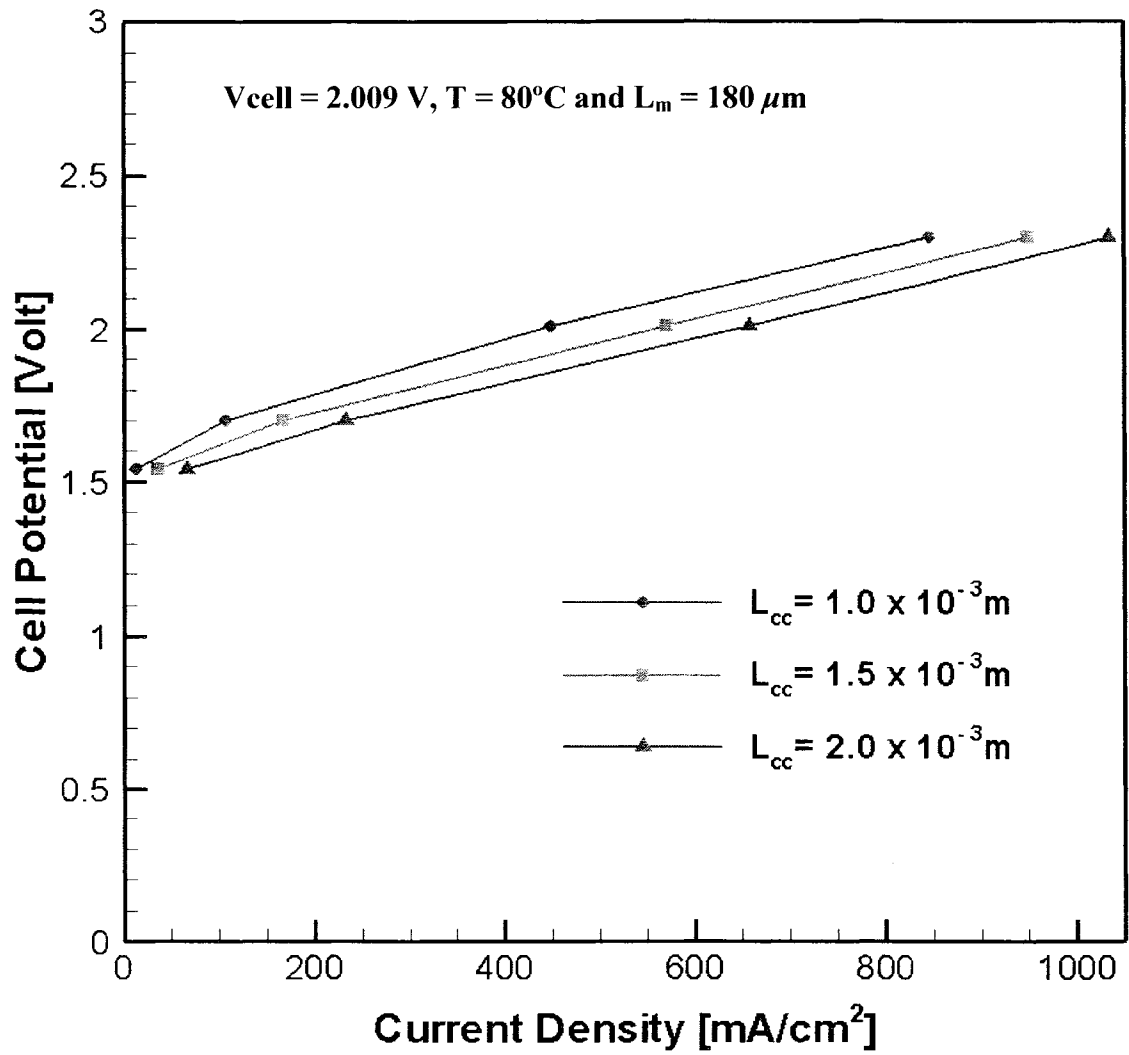
density relation (*i-V* curve)

60

Figure 3.10: Influence of various lengths of current collector on the cell potential vs. Current density relation (*i-V* curve)

CHAPTER 4

CONCLUSIONS AND RECOMMENDATIONS FOR FUTURE WORK

4.1 Conclusions

Numerical modeling has been performed to study the performance and inherent mechanisms of PEM electrolyzer cell in this thesis. The conclusions pertaining to this research work are summarized below as follows:

- The unit mass fraction of water at the inlet passages of the anode and cathode sides, a cell potential of 2.009V and a cell temperature of 80°C have been applied as the operating conditions of the model. The average value of water mass fraction at the anode side outlet is 0.497. The reduction in mass fraction corresponds to the consumption of water during splitting of water molecules in the reaction at anode. The water mass fraction at the cathode side is not involved in the water splitting reaction; instead it is only used for hydrating the thin permeable membrane.

- The oxygen mass fraction applied at the anode inlet is zero. As the water splitting reaction occurs the oxide ions oxidize to form oxygen gas, this corresponds to an increase in the oxygen mass fraction from inlet to outlet passages of the anode. An average value of 0.421 is obtained at the outlet of anode. The mass fraction of

62

oxygen is high at the upper corner of the current collector and its magnitude at that location is 0.584.

- There is zero mass fraction of hydrogen applied at the inlet passage of the feed water and an average value of mass fraction obtained along the boundary of the cathode outlet passage is 0.185. This increase in mass fraction corresponds to the reduction of hydrogen protons into hydrogen gas. The mass fraction of hydrogen gas is high at the upper corner of the current collector and its magnitude at that location is 0.22, while it is 0.41 at the lower corner of the current collector.

- The current density is relatively uniform in the membrane. A decrease in the electric potential is obtained across the membrane from anode side to cathode side.

- Parametric studies have been performed to study the performance of the numerical model and the obtained numerical results have been compared with the available measurement data.

- At constant cell potential, as the temperature of the cell increases, a corresponding increase in the current density values across the cell is obtained.

- As the thickness of the thin permeable membrane is increased, a corresponding decrease in the current density values across the cell is obtained.

- As the length of the current collectors is increased, the current density values across the cell increases and this is because of the increase in the collector area of the cell.

4.2 Recommendations for future research

There are many untouched opportunities to explore in the PEM electrolyzer modeling, although a fundamental modeling framework and considerable understanding have been established in the present work. Such areas include:

- A two-dimensional non-isothermal model can be developed.

- Non-uniform mesh can also be applied to the current numerical model because finer mesh at the boundaries results in more accurate values.

- The influence of photon energy from sunlight can be incorporated in the current model and several parametric effects can be performed on this model.

- A three dimensional modeling of the PEM electrolyzer cell is needed to be performed since it represents the actual conceptual design.

- Furthermore experimental and numerical studies in the catalyst reactive boundaries, protons crossover and hydrogen reduction in the cathode side have to be performed.

- Thermal management should be modeled for stack of PEM electrolyzer cells.

4.2.1 Influence of sunlight on two-dimensional electrolyzer model

The influence of photon energy from sunlight has not been considered in the present model so far. Here, the light-absorbing semiconductor is either the anode or cathode (or both) in an electrochemical cell. The reactions at the junction of a semiconductor material and a liquid, convert solar irradiance into stored chemical energy or electricity. We can further evaluate the performance, stability, and conversion (sunlight to hydrogen) efficiency of this cell. With a band gap of about 2.5 eV and a

demonstrated resistance to photo-corrosion in aqueous solutions, tungsten trioxide (WO_3) thin-films are well matured for photo-anode applications in these water-splitting systems. In order to split water, the semiconductor must meet three simultaneous conditions [51].

1. The first is that the semiconductor must be stable in aqueous solution during hydrogen evolution.

2. The second is that the conduction and valence band edges of the semiconductor overlap the water redox potentials.

3. The third is that charge transfer from the semiconductor to the water occurs quickly.

4.2.2 A three-dimensional model of the electrolyzer cell

Accordingly, a three dimensional, two-phase and multi-component model is to be developed to study the performance of the cell and compare it with the experimental results. The model consists of a complete set of governing equations for all the components that couples the flow, species, potential and current density distribution in the two channel flows, two water diffusion later, two catalyst reactive boundaries and the membrane respectively. Liquid and gas phases are considered in the entire electrode subdomains and only liquid phase in the membrane subdomain. The model can predict the oxygen mole fraction in the anode side, the hydrogen mole fraction in the cathode side, the current and the potential field distribution in the cell. The model should also give attention to the flow of protons through the membrane of the cell.

4.2.3 Thermal management

In the previous chapters, it has been of primary interest to develop a systematic numerical model and identify the major electrochemical and transport phenomena. For a single cell modeling, it is widely assumed that the electrolyzer cell is isothermal. Therefore, no attention has been given to solve the energy equation or study the temperature distribution in PEM electrolyzer cells. However, thermal modeling is important for these stacks of cells.

Two pieces of information are additionally needed in order to include a thermal model in the present numerical model. They are: (1) thermal properties of various materials such as the electrolyte, the water diffusion layer and the contact thermal resistance between the diffusion layer and the current collector; and (2) thermal boundary conditions.

Hence, an effort is needed to couple the energy conservation equation to the numerical model developed and also include the effect of heat sources to simulate more accurately the steady state electrolyzer cell temperature.

66

REFERENCES

1. W. S. Peirce, Economics of the energy industries (2nd ed.), West port, CT: Praeger, 1996.

2. T. N. Veziroglu, Quarter century of hydrogen movement 1974-2000, International Journal of Hydrogen Energy, 25, 1143-1150, 2000.

3. F. Kreith, Fallacies of a hydrogen economy: A critical analysis of hydrogen production and utilization, Journal of Energy Resources Technology, 126, 249–257, 2004.

4. Scott Charles Warren, "Improving efficiency in solar-powered water splitting", MS Thesis, 2002.

5. www.hydrogensolar.com

6. www.hyrogennow.org

7. Joseph Dee Beach Jr., $In_xGa_{1-x}N$ for photoelectrochemical water splitting, MS Thesis, Colorado School of Mines, 2001.

8. Shyam S. Kocha and John A. Turner, Displacement of the bandedges of GaInP2 in aqueous electrolytes induced by surface modification, Journal of the Electrochemical Society 142, 2625-2630, 1995.

9. M. F.Weber and M. J. Dignam, Splitting water with semiconducting photo-electrodes efficiency considerations, International Journal of Hydrogen Energy 11, 225-232, 1986.

10. James R. Bolton, Stewart J. Strickler, and John S. Connolly, Limiting and realizable efficiencies of solar photolysis of water, Nature 316, 495-500, 1985.

11. J. G. Mavroides, D. I. Tchernev, J. A. Kafalas, and D. F. Kolesar, Photoelectrolysis of water in cells with TiO_2 anodes, Materials Research Bulletin, 10, 1023-1030, 1975.

12. Mark S. Wrighton, Arthur B. Ellis, Peter T. Wolczanski, David L. Morse, Harmon B. Abrahamson, and David S. Ginley, Strontium titanate photo-electrodes: efficient photo-assisted electrolysis of water at zero applied potential, Journal of the American Chemical Society, 98, 2774-2779, 1976.

13. J. G. Mavroides, J. A. Kafalas, and D. F. Kolesar, Photoelectrolysis of water in cells with $SrTiO_3$ anodes, Applied Physics Letters, 28, 241-243, 1976.

14. E. Aharon-Shalom and Adam Heller, Journal of the Electrochemical Society, 129, 2865, 1982.

15. Adam Heller, Hydrogen-evolving solar cells, Science, 223, 1141-1148, 1984.

16. Shyam S. Kocha, John A. Turner, and A. J. Nozik, Study of the Schottky barrier and determination of the energetic positions of band edges at the n-type and p-type gallium indium phosphide electrode-electrolyte interface, Journal of Electroanalytical Chemistry, 367, 27-30, 1994.

17. Oscar Khaselev and John A. Turner, Monolithic photovoltaic-photoelectrochemical device for hydrogen production via water splitting, Science, 280, 425-427, 1998.

18. Ioannis Papagiannakis, Studying and Improving the Efficiency of Water Electrolysis using a Proton Exchange Membrane Electrolyzer, MS Thesis, 2005.

19. O. Ulleberg, Modeling of advanced alkaline electrolyzers: a system approach, J of hydrogen energy, Vol. 28, 21 – 33, 2003.

20. www.pege.org/greenwinds/electrolyzer.html

21. J. Divisek, Water electrolysis in a low and medium temperature regime Electrochemical Hydrogen Technologies, 137, 1990.

22. P. Millet, M. Pineri, R. Durand, New solid polymer electrolyte composites for water electrolysis, Journal of Applied Electrochemistry, 19, 162-166, 1989.

23. Y. Nishimura, K. Yasuda, Z. Siroma, K. Asaka, High current density solid polymer electrolyte water electrolysis, Denki kagaku oyobi kogyo butsuri kagaku, 65, 1122-1123, 1997.

24. S. Zhigang, Y. Baolian and H. Ming, Bifunctional electrodes with a thin catalyst layer for 'unitized' proton exchange membrane regenerative fuel cell, Journal of Power Sources, 84, 82-85, 1999.

25. T. Ioroi, N. Kitazawa, K. Yasuda, Y. Yamamoto and H. Takenaka, Iridium oxide/Platium electrocatalysts for utilized regenerative polymer electrolyte fuel cells, Journal of the Electrochemical Society, 147, 2018- 2022, 2000.

26. J. Sedlak, R. Lawrence and J. Enos, Advances in oxygen evolution catalysis in solid polymer electrolyte water electrolysis, International Journal of Hydrogen Energy, 6, 159-165, 1981.

27. H. Takenaka, E. Torikai, Y. Kawami and N. Wakabayashi, Solid polymer electrolyte water electrolysis, International Journal of Hydrogen Energy, 7, 397-403, 1982.

28. P. Millet, R. Durand and M. Pineri, Preparation of new solid polymer electrolyte composites for water electrolysis, International Journal of Hydrogen Energy, 15, 245-253, 1990.

29. P. Millet, F. Andolfatto and R. Durand, Design and performance of a solid polymer electrolyte water electrolyzer, International Journal of Hydrogen Energy, 21, 87-93, 1996.

30. E. Rasten, Electrocatalysis in water electrolysis with solid polymer electrolyte, PhD Thesis, NTNU Trondheim, 2001.

31. M. Yamaguchi, K. Yagiuchi and K. Okisawa, R&D of high performance solid polymer electrolyte water electrolyzer in WE-NET, Hydrogen Energy Progress XI, Proceedings of the World Hydrogen Energy Conference, 781-786, 1996.

32. M. Nagai, H. Tazima, A. Sakanishi, N. Hisatome and S. Ohkura, Development on solid polymer electrolyte water electrolysis technology for high current density and energy efficiency, Hydrogen Energy Progress XI, Proceedings of the World Hydrogen Energy Conference, 825-830, 1996.

33. M. Yamaguchi, K. Okisawa and T. Nakanori, Development of high performance solid polymer electrolyte water electrolyzer in WE-NET, Proceedings of the Intersociety Energy Conversion Engineering Conference 32nd, 1958-1965, 1997.

34. M. Yamaguchi, T. Shinohara, H. Taniguchi, T. Nakanori and K. Okisawa, Development of 2500cm^2 solid polymer electrolyte water electrolyzer in WE-NET, Hydrogen Energy Progress XII, Proceedings of the World Hydrogen Energy Conference, 747-755, 1998.

35. S. Grigor'ev, M. Khaliullin, N. Kuleshov and V. Fateev, Electrolysis of water in a system with a solid polymer electrolyte at elevated pressure, Russian Journal of Electrochemistry (Translation of Elektrokhimiya), 37, 819-822, 2001.

36. K. Ledjeff, F. Mahlendorf, V. Peinecke and A. Heinzel, Development of electrode membrane units for the reversible polymer fuel cell (RSPFC), Electrochimca Acta, 40 315-319, 1995.

37. P. Millet, Water electrolysis using EME technology: electric potential distribution inside a nafion membrane during electrolysis, Electrochimica Acta, 2501-2506, 1994.

38. S. Stucki and A. Menth, Proc. Symp. Industrial water electrolysis, ECS series, Princetown, NJ, p. 180, 1978.

39. J. MacBreen, J. electrochem. Soc, 132, 1112, 1985.

40. Onda. K, Murakami. T, Hikosaka. T, Kobayashi. M, Notu. R and Ito. K, 2002, Performance analysis of polymer electrolyte water electrolysis cell at a small-unit test cell and performance prediction of large stacked cell, Journal of the Electrochemical Society, 149 (8), pp. A1069-A1078.

41. Choi, P., Bessarabov, D. G. and Datta, R., 2004, A simple model for solid polymer electrolyte (SPE) water electrolysis, Solid State Ionics, 175, pp. 535-539.

42. Nie, J. H., Katukota, S. P., Chen, Y. T., Boehm, R. F. and Hsieh, H. T., A photo-electrochemical model of solid polymer water electrolysis for hydrogen production from sunlight, 1st Energy Nanotechnology International Conference, ENIC2006-19039, Massachusetts Institute of Technology (MIT), Cambridge, MA, USA, June 26-28, 2006.

43. Katukota, S. P., Nie, J. H., Chen, Y. T., Boehm, R. F. and Hsieh, H. T., "Numerical Investigation for Hydrogen Production using Proton Exchange Water Electrolysis cell", Comsol Users Conference, Las Vegas, NV, USA, October 26-27, 2006.

44. www.bioanalytical.com/products/ec/faqele.html

45. T. Berning, D. M. Lu, and N. Djilali, Three-dimensional computational analysis of transport in a PEM fuel cell, Journal of Power Sources,106, 284-294, 2002.

46. A.J. Bard, and L.R. Faulkner, Electrochemical Methods, Wiley, New York, 1980.

47. T. Berning and N. Djilali, Three-dimensional computational analysis of transport phenomena in a PEM fuel cell – a parametric study, Journal of Power Resources 124,440-452, 2003.

48. S. Um and C. Y. Wang, Three-dimensional analysis of transport and electrochemical reactions in polymer electrolyte fuel cells, Journal of Power Sources,125, 40-51, 2004.

49. G. H. Guvelioglu and H. G. Stenger, Computational fluid dynamics modeling of polymer electrolyte membrane fuel cells, Journal of Power Sources,147, 95-106, 2005.

50. www.h-tec.com

51. www.answers.com/topic/electrolysis

52. COMSOL 3.2 User Guide, COMSOL Inc., Burlington, MA, 2004.

53. R.B. Bird, W.E. Stewart, and E.N. Lightfoot, Transport Phenomena, Wiley, 2nd edition, New York, 1960.

VITA

Graduate College
University of Nevada, Las Vegas

Shanthi P Katukota

Local Address:
935 East Cottage Grove Avenue, Apt 35,
Las Vegas, NV 89119

Permanent Address:
73 Rachel Court,
Franklin Park, New Jersey 08823

Degree:
Bachelor of Engineering, Mechanical Engineering, 2004
Osmania University, Hyderabad, AP, India

Thesis Title:
Computational Modeling of Proton Exchange Membrane Electrolysis cell
for Hydrogen Production

Publications:
Katukota, S. P., Nie, J. H., Chen, Y. T., Boehm, R. F. and Hsieh, H. T., "A photo-electrochemical model of solid polymer water electrolysis for hydrogen production from sunlight," 1st Energy Nanotechnology International Conference, ENIC2006-19039, Massachusetts Institute of Technology (MIT), Cambridge, MA, USA, June 26-28,2006.

Katukota, S. P., Nie, J. H., Chen, Y. T., Boehm, R. F. and Hsieh, H. T., "Numerical Investigation for Hydrogen Production using Proton Exchange Water Electrolysis cell", Comsol Users Conference, Las Vegas, NV, USA, October 26-27, 2006.

Thesis Examination Committee:
Chair Person, Dr. Yitung Chen, Ph. D.
Committee Member, Dr. Robert Boehm, Ph. D.
Committee Member, Dr. Jianhu Nie, Ph. D.
Graduate Faculty Representative, Dr. Satish C Bhatnagar, Ph. D.

73